

Stochastic dynamics of adhesion clusters under shared constant force and with rebinding

Thorsten Erdmann and Ulrich S. Schwarz

Max Planck Institute of Colloids and Interfaces, 14424 Potsdam, Germany

(Received 12 May 2004; accepted 18 August 2004)

Single receptor-ligand bonds have finite lifetimes, so that biological systems can dynamically react to changes in their environment. In cell adhesion, adhesion bonds usually act cooperatively in adhesion clusters. Outside the cellular context, adhesion clusters can be probed quantitatively by attaching receptors and ligands to opposing surfaces. Here we present a detailed theoretical analysis of the stochastic dynamics of a cluster of parallel bonds under shared constant loading and with rebinding. Analytical solutions for the appropriate one-step master equation are presented for special cases, while the general case is treated with exact stochastic simulations. If the completely dissociated state is modeled as an absorbing boundary, mean cluster lifetime is finite and can be calculated exactly. We also present a detailed analysis of fluctuation effects and discuss various approximations to the full stochastic description. © 2004 American Institute of Physics.

[DOI: 10.1063/1.1805496]

I. INTRODUCTION

Cells in a multicellular organism adhere to each other and to the extracellular matrix through a large variety of different receptor-ligand bonds.¹ Although not probed this way in traditional affinity experiments, adhesion bonds in physiological situations usually have to function under mechanical load. For example, cell-matrix adhesion in connective tissue is mainly provided by focal adhesions, which are based on transmembrane receptors from the integrin family connecting the actin cytoskeleton to the extracellular matrix. Focal adhesions of fibroblasts, the main cell type in connective tissue, are usually loaded by actomyosin contractility, in particular, during tissue maintenance and wound healing. An important class of adhesion contacts in endothelial sheets are adherens junctions, which are based on transmembrane receptors from the cadherin family connecting the actin cytoskeletons of different cells. Endothelial tissue often is subjected to considerable external stress and strain, for example, in lung and blood capillaries. Leukocytes circulating with the blood flow tether to and roll on vessel walls through transmembrane receptors from the selectin family connecting the actin cytoskeleton to carbohydrate ligands on the opposing surface. Here contact dissociation is accelerated due to the shear flow pulling on the cells. In general, there are many more physiological conditions in which adhesion clusters are subject to forces arising from intracellular or extracellular processes, including cell motility, development, and angiogenesis.

During recent years, the behavior of different adhesion bonds under force has been investigated extensively on the level of single molecules by dynamic force spectroscopy.²⁻⁴ This field has been pioneered by AFM experiments by Gaub and co-workers⁵ and later put onto a firm theoretical basis by Evans and Ritchie.⁶ Because bond rupture can be modeled in the framework of Kramers theory as thermally assisted escape over one or several transition state barriers, bond

strength is a dynamic quantity which depends on loading rate. Experimentally, this prediction has been impressively confirmed for different molecular systems.⁷⁻¹⁰ Dynamic force spectroscopy has been implemented with different experimental techniques, including atomic force microscopy,⁷ laser optical tweezers,⁸ and the biomembrane force probe.^{9,10} The behavior of molecular bonds under force can also be probed in parallel plate flow chambers. Here usually the loading process is much faster than bond dissociation, which therefore effectively occurs under constant load.^{11,12} By now, dynamic force spectroscopy has shown that adhesion bonds feature a much more complicated behavior under force than suggested by the traditional affinity experiments in solution.¹³ Using concepts from the theory of stochastic dynamics,^{6,14-17} a binding energy landscape can be reconstructed from the experimental data. During recent years, this has been accomplished for many different adhesion receptors, including integrins,^{18,19} cadherins,²⁰ and selectins.^{21,22} However, while dynamic force spectroscopy up to now has mainly been applied to single bonds, in physiological settings adhesion receptors usually operate cooperatively within clusters.²³ Therefore the physical description of single adhesion bonds under force now has to be extended to clusters of adhesion bonds under force. Clusters also open up the possibility of rebinding of broken bonds, which is known to be essential to achieve physiological lifetimes of adhesion clusters. For single bonds, rebinding usually cannot be studied due to elastic recoil of the force transducer after bond rupture.² In contrast, for adhesion clusters open bonds can rebind as long as other bonds are closed, thus keeping the spatial proximity required for rebinding. Only if the completely dissociated state is reached, rebinding becomes impossible and the cluster disintegrates as a whole.

Although it is clear that force leads to accelerated cluster dissociation, it is usually not known how it is distributed over the different closed bonds in different situations of

interest. In many cases, most prominently in rolling adhesion, only few of the different bonds are loaded to an appreciable degree, thus dissociation occurs in a peeling fashion.^{24–26} However, due to geometrical reasons, even in this case there will be a subset of bonds which are loaded to a similar extent. In the same vein, the loading situation at focal adhesions can also be expected to be rather complicated. For the case of homogeneous loading, one further has to distinguish between loading through soft and stiff springs.²⁷ In the latter case, all bonds are equivalent and a mean field description can be applied.²⁸ In the first case, force is shared equally between all closed bonds and the coupling between the different bonds in the adhesion cluster is nontrivial. Recently, dynamic force spectroscopy has been applied to this case for the first time.²⁹ Here, a vesicle functionalized with appropriate ligands is sucked into a micropipette and pressed onto a cell. On retraction, the vesicle is peeled off from the outside to the inside of the contact region. However, due to rotational symmetry around the micropipette axis, all bonds in a ring around the periphery of the contact area share the homogeneous loading.

The equilibrium properties of adhesion clusters has been theoretically studied before,^{23,30–32} mainly in reference to experiments on vesicle adhesion through specific ligand-receptor pairs.^{33–35} For the nonequilibrium dissociation of adhesion clusters under force, a deterministic model has been introduced in a seminal paper by Bell.²³ This model has been mainly used to study more specific problems, for example, leukocyte rolling in shear flow.³⁶ Recently, the deterministic Bell model has also been extended to treat linear loading of a cluster of adhesion bonds, which usually is applied in dynamic force spectroscopy.^{27,28} A stochastic version of the Bell model has been introduced, but studied only in the large system limit and for specific parameter values.³⁷ Later the stochastic model has been treated with reliability theory in the special case of vanishing rebinding.³⁸ Other special cases of the stochastic model have been treated in order to evaluate specific experiments, for example the binding probability between ligands and receptors on opposing surfaces as a function of contact time.^{34,39}

In this paper, we use the stochastic version of the Bell model to study the case of constant shared loading in comprehensive detail. In contrast to applications to specific experiments, we focus on generic features of the stochastic dynamics of a cluster of parallel bonds under shared constant loading and with rebinding. A short report on our main results has been given before.⁴⁰ As shown elsewhere, the same stochastic framework as used here for the case of constant loading can also be used to study the case of linear loading.⁴¹ Compared with the deterministic model, the stochastic model has several advantages: first, only the stochastic model allows to treat the experimental situation that rebinding becomes impossible once the completely dissociated state has been reached. Second, it includes fluctuations and nonlinear effects, which are important for small adhesion clusters. Third, using the well-developed theory on master equations, the stochastic model allows to derive analytical results for cluster lifetime as a function of cluster size, rebinding rate

and force, which are very helpful in evaluating adhesion experiments, including rolling adhesion.⁴²

In the following, we consider the situation in which a certain number of bound adhesion receptors has been clustered and connected to some force-bearing structure. We then ask how strongly the force accelerates dissociation, and in which sense dissociation can be balanced by rebinding. Since we are concerned with generic features of contact stability, our model does not consider spatial or concentration degrees of freedom. In Sec. II, we define the stochastic variant of the deterministic Bell model, which has three dimensionless parameters. Next we introduce the appropriate one-step master equation describing the stochastic dynamics of an adhesion cluster under shared constant force and with rebinding. We also explain how this master equation can be solved numerically with the Gillespie algorithm for exact stochastic simulations. In the two following sections, we discuss two special cases of the model in which considerable analytical progress can be made. In each case, we first discuss deterministic results, and then turn to the full stochastic model. In Sec. III, we discuss the case of vanishing rebinding. In this case, broken bonds cannot be reformed and the number of closed bonds in the adhesion clusters decreases in a unique sequence of rupture events. This can be used to construct a solution for the master equation and to derive an expression for the average lifetime of an adhesion clusters. In Sec. IV, we discuss the case of vanishing force. In this case, we deal with a linear problem and analytical solutions of the master equation can be derived for a reflecting boundary. They can be used in turn to derive an approximation for the case with an absorbing boundary. Cluster lifetime can be calculated exactly as mean first passage time using Laplace techniques. In Sec. V we consider the general case with finite rebinding and finite force. Although full analytical solutions are only feasible in the case of small clusters, cluster lifetime can be calculated exactly for arbitrary cluster size. For larger clusters, full solutions of the master equation are obtained by exact stochastic simulations. Simulations are also essential to characterize single unbinding trajectories and to understand the role of fluctuations. We close in Sec. VI with a discussion of experimental issues.

II. MASTER EQUATION

A. Derivation

The rupture of molecular bonds can be modeled in the framework of Kramers theory as thermally activated escape over a transition state barrier.^{6,14,15} Assuming an infinitely sharp transition state barrier leads to the so-called *Bell equation* for the single molecule dissociation rate as a function of force, $k = k_0 e^{F/F_b}$.²³ Here the force scale $F_b = k_B T / x_b$ is set by thermal energy $k_B T$ and the distance x_b between the potential minimum and the transition state barrier along the reaction coordinate of rupture. For a typical value $x_b \approx 1$ nm and physiological temperature $T \approx 300$ K, we find the typical force scale $F_b \approx 4$ pN. Physiological loading has indeed been found to be in the pN-range, both for cell-matrix adhesion^{43–45} and rolling adhesion.^{11,46} Values for k_0 and F_b have been measured during recent years with dynamic force

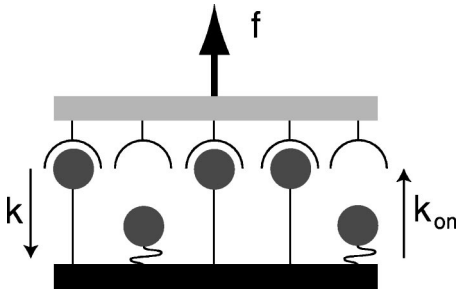


FIG. 1. Schematic representation of an adhesion cluster under constant shared force: there are $N_t=5$ receptor-ligand pairs, $i=3$ of which are closed and equally share the load f . A closed bond ruptures with the dissociation rate $k=k_0e^{f/i}$. The $N_t-i=2$ open bonds rebind with the force-independent association rate k_{on} . Our model has three parameters: cluster size N_t , dimensionless rebinding rate $\gamma=k_{on}/k_0$ and dimensionless force f .

spectroscopy for different receptor-ligand systems, including integrins,^{18,19} cadherins,²⁰ and selectins.^{21,22} While the dissociation rate k depends mainly on the internal structure of a bond, the association rate k_{on} includes the formation of an encounter complex and therefore depends on the details of the situation under consideration. It is very difficult to determine k_{on} experimentally, especially in the case of cell adhesion, when the interacting molecules are anchored to opposing surfaces.^{34,39,47} In order to focus on the generic features of cluster stability, here we assume that k_{on} is a force-independent constant, in accordance with earlier theoretical work.^{23,27,36,37} Future modeling might refine this assumption, considering for example the effect of ligand-receptor separation controlled by polymeric tethers.⁴⁸⁻⁵⁰

For the following, it is convenient to use dimensionless quantities. We define dimensionless time $\tau=k_0t$, dimensionless force $f=F/F_b$ and dimensionless rebinding rate $\gamma=k_{on}/k_0$. The dimensionless single molecule dissociation rate is $k/k_0=e^f$. We consider a cluster with a constant number of N_t bonds, which initially are all closed and then undergo rupture and rebinding according to the appropriate rates (Fig. 1). Since bond rupture is a discrete process, the stochastic dynamics of the bond cluster can be described by the one-step master equation⁵¹

$$\frac{dp_i}{d\tau} = r_{i+1}p_{i+1} + g_{i-1}p_{i-1} - [r_i + g_i]p_i, \quad (1)$$

where $p_i(\tau)$ is the probability that i bonds are closed at time τ . Here the r_i and g_i are the reverse and forward rates between the possible states i ($0 \leq i \leq N_t$). They follow from dissociation and association rates of single bonds as

$$r_i = r(i) = ie^{f/i} \quad (2a)$$

and

$$g_i = g(i) = \gamma(N_t - i). \quad (2b)$$

Our model has three parameters, namely, cluster size N_t , rebinding rate γ , and force f . Since $i \geq 0$ should be guaranteed at any time, $r_0=0$ has to be set for $f > 0$, in addition to the definitions in Eq. (2). Moreover, Eq. (2) implies $g_0 > 0$, that is, after rupture of the last closed bond new bonds are allowed to form. This corresponds to a reflecting boundary of

the master equation at $i=0$. As explained above, in biological and biomimetic situations rebinding of the completely dissociated state is usually prevented by elastic recoil of the transducer. Therefore in the following we set $g_0=0$ in order to model an absorbing boundary at $i=0$. Because the values for r_0 and g_0 do not follow the general form given in Eq. (2), the boundary at $i=0$ is an *artificial* boundary. Concerning the upper end of the set of states at $i=N_t$, the form $g_{N_t}=0$ represents a reflecting boundary and guarantees $i \leq N_t$. Thus, the upper boundary is a *natural* boundary of the master equation.

A quantity of large interest is the average number of closed bonds $N(\tau) = \langle i \rangle = \sum_{i=1}^{N_t} ip_i(\tau)$. From the master equation Eq. (1) one can derive⁵²

$$\frac{dN}{d\tau} = \sum_{i=0}^{N_t} i \frac{dp_i}{d\tau} = -\langle r(i) \rangle + \langle g(i) \rangle. \quad (3)$$

If $r(i)$ and $g(i)$ were both linear functions in i , Eq. (3) would become an ordinary differential equation for N . This suggests to study the deterministic equation

$$\frac{dN}{d\tau} = -r(\langle i \rangle) + g(\langle i \rangle) = -Ne^{f/N} + \gamma(N_t - N) \quad (4)$$

as has been done by Bell.²³ Below we will see that the analysis of this equation gives valuable insight into the generic features of our model. However, it is important to note that for $f > 0$, the reverse rate $r(i)$ in Eq. (2) is nonlinear in i and the average in Eq. (3) cannot be taken. Instead lower moments are related to higher moments and one arrives at a complicated hierarchy of coupled differential equations. The solution of the deterministic equation Eq. (4) will therefore deviate from the average number of closed bonds obtained from the solution of the master equation Eq. (1). The same problem arises for the higher moments. For example, for the variance $\sigma_N^2 = \langle i^2 \rangle - \langle i \rangle^2$ one can derive⁵²

$$\frac{d\sigma_N^2}{dt} = \langle g(i) + r(i) \rangle + 2\langle (i - \langle i \rangle)[g(i) - r(i)] \rangle, \quad (5)$$

where again the average cannot be taken. As an approximate treatment, one can expand $r(i)$ in a Taylor series around the average for i , $\langle i \rangle = N$.⁵¹ Restricting the expansion to second order, thus assuming a Gaussian distribution, leads to the following equations:

$$\frac{dN}{d\tau} = -Ne^{f/N} + \gamma(N_t - N) - \sigma_N^2 e^{f/N} \frac{f^2}{2N^3}, \quad (6)$$

$$\frac{d\sigma_N^2}{d\tau} = Ne^{f/N} + \gamma(N_t - N) - \sigma_N^2 \left[e^{f/N} \left(2 - \frac{2f}{N} - \frac{f^2}{2N^3} \right) + \gamma \right]. \quad (7)$$

In principle, these equations can be solved by numerical integration. However, it is much more instructive to consider the original master equation. Moreover, the deterministic equation Eq. (4) and its improved version Eq. (6) cannot describe the effect of an absorbing boundary at $i=0$. In order to consider this experimentally relevant case, one has to

study the master equation Eq. (1) with the rates given in Eq. (2). Finally, only the full stochastic analysis reveals the detailed effect of fluctuations.

B. Numerical solution

Below we will present analytical solutions for several special cases of the master equation. In the general case, we numerically solve the master equation by Monte Carlo methods. In detail, for each set of parameter values N_t , f , and γ , we generate between 10^4 and 10^6 trajectories with the help of the Gillespie algorithm for exact stochastic simulations.^{53,54} By averaging for given time τ over the different simulation trajectories, we obtain the desired probability distributions $\{p_i(\tau)\}_{i=0}^{N_t}$. In general it is also rather instructive to study single simulation trajectories, because their specific features are expected to be characteristic also for experimental trajectories.

The Gillespie algorithm was originally developed for exact simulation of the stochastic dynamics of coupled chemical reactions. Applied to our case, open and closed bonds correspond to two different species of molecules and the transition between these two species, that is, rupture and rebinding, correspond to chemical reactions. The Gillespie algorithm is very efficient because rather than discretizing time in small steps, it generates jumps between subsequent reactions. The basic quantity of the Gillespie algorithm is the probability $P(\mu, \tau | \tau_0, X) d\tau$ that the next reaction occurs in the time interval $[\tau_0 + \tau, \tau_0 + \tau + d\tau]$ and is of type μ under the condition that at time τ_0 the system is in state X . In our case, μ has only two values corresponding to rupture and rebinding, and the state X of the system is completely described by the number of closed bonds i . Since the rupture and rebinding rates from Eq. (2) are constant between subsequent events, P does not depend on absolute time τ_0 . In fact it reads

$$P(\mu, \tau | \tau_0, X) = P(\mu, \tau | i) = P_0(\tau | i) a_\mu, \quad (8)$$

where P_0 is the probability that no reaction occurs in the time interval $[0, \tau]$ and a_μ is the reaction rate for reaction μ . P_0 satisfies the differential equation

$$\frac{dP_0}{d\tau} = - \left(\sum_{\mu} a_{\mu} \right) P_0, \quad (9)$$

and the initial condition $P_0(0) = 1$, therefore $P_0(\tau | i) = e^{-(\sum_{\mu} a_{\mu})\tau}$. $P(\mu, \tau | i)$ is properly normalized to unity as can be shown by integrating over time and summing over reactions. The Gillespie algorithm generates trajectories in which subsequent reactions are separated by the following rule. In the absence of other reactions, the probability for a reaction μ in the time interval $[\tau, \tau + d\tau]$ is given by

$$p_{\mu}(\tau) = a_{\mu} e^{-a_{\mu}\tau} d\tau. \quad (10)$$

The integral

$$F_{\mu}(\tau) = \int_0^{\tau} p_{\mu}(\tau') d\tau' = 1 - e^{-a_{\mu}\tau} \quad (11)$$

is the probability for a reaction occurring until time τ . It increases strictly monotonically from 0 to unity and thus can

be inverted. In order to generate a random variable τ_{μ} which is distributed according to Eq. (10), one generates a random number ξ which is uniformly distributed over the interval $[0, 1]$ and inserts it into the formula

$$\tau_{\mu} = - \frac{\ln(\xi)}{a_{\mu}}. \quad (12)$$

This is done for each type of reaction, leading to a set of times τ_{μ} . The time for the next reaction is then chosen as the smallest τ_{μ} , that is, $\tau = \min_{\mu}(\tau_{\mu})$. As shown in Refs. 53 and 54, this rule generates trajectories with the correct distribution of times and types of subsequent reactions. With the forward and reverse rates Eq. (2) for rebinding and unbinding of molecular bonds in the cluster, the random times are determined by the functions

$$\tau_f = - \frac{\ln(\xi)}{\gamma(N_t - i)} \quad (13a)$$

and

$$\tau_r = - \frac{\ln(\xi)}{i e^{f/i}}. \quad (13b)$$

This algorithm is exact in the sense that the only sources of inaccuracy lie in the choice of the random number generator and the finite number of trajectories used to calculate probability distribution.

III. VANISHING REBINDING

A. Deterministic analysis

We start our analysis with the case of vanishing rebinding, $\gamma = 0$. Then the deterministic equation Eq. (4) reads

$$\frac{dN}{d\tau} = -N e^{f/N}. \quad (14)$$

In principle, the total number of bonds N_t is irrelevant in this case. However, it is reintroduced through the initial condition $N(0) = N_t$. Then Eq. (14) is solved implicitly by²³

$$\tau(N) = E\left(\frac{f}{N_t}\right) - E\left(\frac{f}{N}\right), \quad (15)$$

where $E(z) = \int_z^{\infty} dz' e^{-z'}/z'$ is the exponential integral. Unfortunately, the inversion for $N(\tau)$ is not possible in general.

In the deterministic description, cluster lifetime T_{det} can be identified with the time τ at which only one last bond exists. Setting $N(T_{\text{det}}) = 1$ in Eq. (15) gives

$$T_{\text{det}} = E\left(\frac{f}{N_t}\right) - E(f). \quad (16)$$

From this result, we can extract three different scaling regimes. For small force, $f < 1$, we use the small argument expansion of the exponential integral, $E(z) \approx -\Gamma - \ln(z)$ (where $\Gamma = 0.577$ is the Euler constant), and find

$$T_{\text{det}} \approx \ln N_t. \quad (17)$$

This corresponds to the familiar case of radioactive decay, when the differential equation $dN/d\tau = -N$ leads to exponential decay $N = N_t e^{-\tau}$.

For intermediate force, $1 < f < N_t$, we can rewrite Eq. (16) for the cluster lifetime as the sum of two integrals,

$$T_{\text{det}} = \int_{f/N_t}^1 dz \frac{e^{-z}}{z} + \int_1^f dz \frac{e^{-z}}{z}. \quad (18)$$

The second integral can be estimated to be $\int_1^f dz (e^{-z}/z) < \int_1^f dz e^{-z} = e^{-1} - e^{-f} < e^{-1}$. For the first integral, we can expand the integrand for small arguments, leading to $\int_{f/N_t}^1 dz (e^{-z}/z) \approx \int_{f/N_t}^1 dz (1-z)/z \approx \ln(N_t/f)$. Since $N_t > f$, the second integral can be neglected and we have

$$T_{\text{det}} \approx \ln\left(\frac{N_t}{f}\right). \quad (19)$$

For the time evolution of the cluster, both exponential integrals in Eq. (15) can be replaced by the small argument approximation as long as $N > f$ and hence the exponential decay proceeds until the force per bond is $f/N = 1$. Thereafter the decay will be faster than exponential due to the destabilizing effect of force.

For large force, $f > N_t$, the second term in Eq. (16) can be neglected and we can use the large argument approximation for the exponential integral, $E(z) \approx e^{-z}/(1+z)$, leading to²³

$$T_{\text{det}} \approx \frac{e^{-f/N_t}}{1+f/N_t}. \quad (20)$$

Therefore cluster lifetime decays faster than exponential with f/N_t in this regime. Now the small argument approximation is not applicable to either of the two terms in Eq. (15) and the decrease in N will be faster than exponential over the whole range of time.

In summary, the analysis of the deterministic equation Eq. (14) allows to identify three scaling regimes of small, intermediate and large force. This analysis also shows that f/N_t is an important scaling variable, which we will therefore use to analyze also the stochastic case.

B. Stochastic analysis

For finite force, $f > 0$, the reverse rate $r(i)$ in Eq. (2) is nonlinear in i and the boundary at $i=0$ is artificial. Therefore the master equation in general cannot be solved with standard techniques. However, in the case of vanishing rebinding, $\gamma=0$, one can use the fact that the decay of the cluster corresponds to a unique sequence of events, with the number of closed bonds decreasing monotonously from N_t to 0. The transition from state i (with i closed bonds present) to the state $i-1$ (with one more broken bond) is a Poisson process with the time-independent rate r_i . If i bonds are present at time τ , the probability that the next bond ruptures at time $\tau + \tau'$ is given by

$$p_{i \rightarrow i-1}(\tau') = r_i e^{-r_i \tau'}. \quad (21)$$

The state probability p_{i-1} is related to the state probability p_i and the transition probability $p_{i \rightarrow i-1}$ by the recursive expression

$$\begin{aligned} p_{i-1}(\tau) &= \int_0^\tau d\tau' p_i(\tau') p_{i \rightarrow i-1}(\tau - \tau') \\ &= r_i e^{-r_i \tau} \int_0^\tau d\tau' p_i(\tau') e^{r_i \tau'}, \end{aligned} \quad (22)$$

which uses the fact that the state $i-1$ can be reached only through the state i . This scheme is solved by

$$p_i(\tau) = \left(\prod_{j=i+1}^{N_t} r(j) \right) \sum_{j=i}^{N_t} \left\{ e^{-r(j)\tau} \prod_{\substack{k=i \\ k \neq j}}^{N_t} \frac{1}{r(k) - r(j)} \right\} \quad (23)$$

as can be shown by induction. The properties of this expression follow from the properties of the reverse rate $r(i) = i e^{f/i}$, which for finite force, $f > 0$, is a nonmonotonous function of i . It diverges for $i \rightarrow 0$, has a minimum at $i = [f]$ (the integer closest to f) and grows as i for $i \rightarrow \infty$. In the unlikely case that the value of f is such that $r(j) = r(k)$ for $j \neq k$, the limit of the expression in Eq. (23) for $r(k) \rightarrow r(j)$ has to be taken carefully. In order to treat this case properly, one has to replace Eq. (23) by

$$\begin{aligned} p_i(\tau) &= \left(\prod_{j=i+1}^{N_t} r(j) \right) \sum_{j=i}^{N_t} \left\{ e^{-r(j)\tau} \left(\prod_{\substack{k=i \\ r(k) \neq r(j)}}^{N_t} \frac{1}{r(k) - r(j)} \right) \right. \\ &\quad \left. \times \left(\prod_{\substack{k=i \\ r(k) = r(j) \\ k \neq j}}^{N_t} \frac{\tau}{2} \right) \right\}, \end{aligned} \quad (24)$$

where we have used $\lim_{\Delta \rightarrow 0} (1 - e^{-\Delta\tau})/\Delta = \tau$ for $\Delta = r(i) - r(k)$. In Fig. 2 we plot the full solution to the master equation, that is, the state probabilities $p_i(\tau)$ from Eq. (23), for $N_t = 10$ and four different values of force f . For small force, all states are appreciably occupied during the decay, that is, each of the curves is a maximum of the set of curves during a certain period of time. In the long run, p_0 approaches unity and all other p_i disappear, because without rebinding, the cluster has to dissociate eventually. For increasing force, the shape of the curves changes considerably. Now the lower states (with small number of closed bonds i) hardly become occupied during the decay process. For very large force, the maximum occupancy changes directly from the initial state N_t over to the detached state 0.

With the help of the exact solution Eq. (23), any quantity of interest can now be calculated. One quantity of large interest is the average number $N(\tau) = \langle i \rangle = \sum_{i=1}^{N_t} i p_i(\tau)$ of closed bonds at time τ . For a single bond, N is simply the probability p_1 that the bond is attached,

$$N(\tau) = p_1(\tau) = e^{-e^f \tau}. \quad (25)$$

For a two-bond cluster we have

$$\begin{aligned} N(\tau) &= p_1(\tau) + 2p_2(\tau) \\ &= \frac{2}{2 - e^{f/2}} \{ e^{-e^f \tau} + (1 - e^{f/2}) e^{-2e^{f/2} \tau} \}. \end{aligned} \quad (26)$$

For increasing N_t , the corresponding expressions become increasingly cumbersome. In general, $N(t)$ is a sum of N_t exponentials with the different relaxation rates $r(i)$ with 1

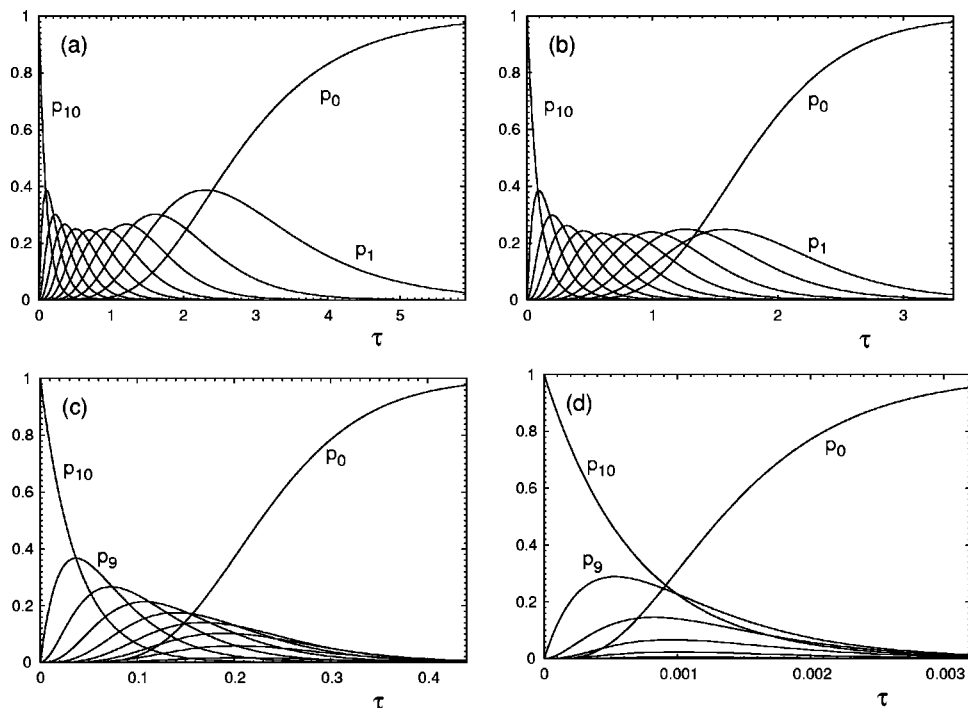


FIG. 2. The state probability $p_i(\tau)$ is the probability that i bonds are closed at time τ ($0 \leq i \leq N_t$). Here the p_i are plotted as a function of time τ for a cluster of initial size $N_t=10$ for $\gamma=0$ and (a) $f=0$, (b) $f=1$, (c) $f=10$, and (d) $f=50$.

$\leq i \leq N_t$. For small force, $f < 1$, $r(i) \approx i$ and the smallest rate corresponds to $i=1$, that is, $N \sim e^{-\tau}$ on large time scales. In this case, clusters of any size decay with the same slope as single bonds and the difference between single and multiple bond rupture lies in the prefactor, not in the time scale of average decay. For intermediate force, $1 < f < N_t$, and large time scales, decay is dominated by $i = [f]$, that is, $N \sim e^{-f\tau}$. Thus the absolute value of force governs the long time behavior, with different sizes showing up only in the prefactor. For large force, $f > N_t$, decay at large time scales is dominated by $i = N_t$, that is, $N \sim e^{-N_t f / N_t \tau}$. This implies that for a given force f , the largest clusters show the slowest decays in the long run. However, if one controls f/N_t rather

than f , the cluster with the smallest size will decay the slowest, since it is subject to the smallest absolute force. In Fig. 3 we plot $\ln N$ as a function of time τ for different values of cluster size N_t and force per initial bond f/N_t . All curves initially show an exponential decay with the rate of a single bond. For small forces decay stays exponential for almost all times. The larger force, the earlier decay crosses over to the late stage regime of superexponential decay.

As noted in Sec. II, due to the nonlinear form of $r(i) = i e^{f/i}$ for $f > 0$, the first moment $N(\tau)$ of the stochastic solution Eq. (23) is not identical with the function $N(\tau)$ obtained from the deterministic equation Eq. (14). In Fig. 4, results for $N(\tau)$ derived from the deterministic and the sto-

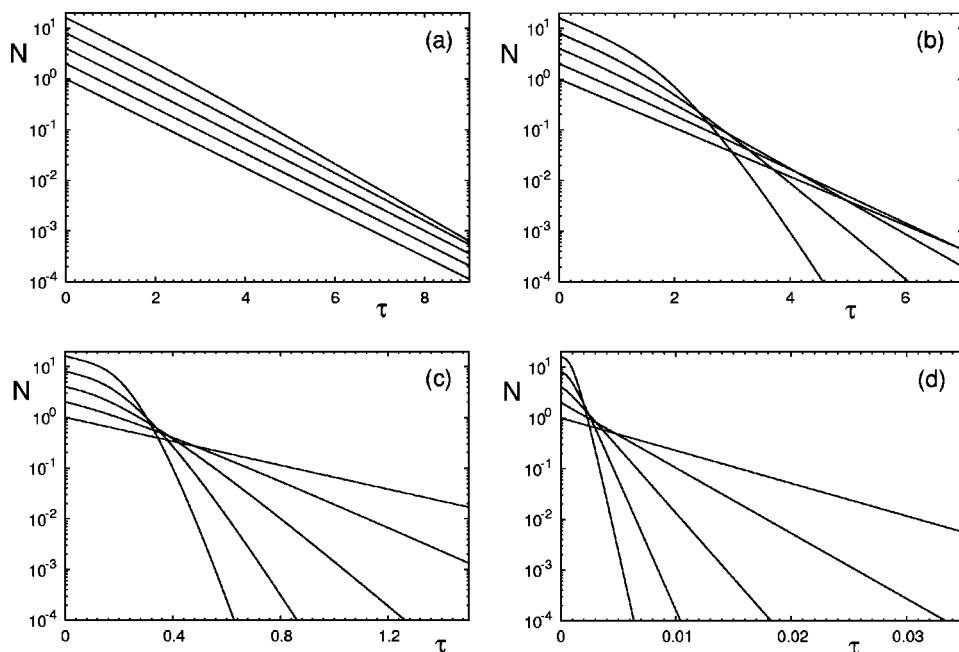


FIG. 3. Average number of closed bonds N as a function of time τ for different cluster sizes $N_t=1, 2, 4, 8$, and 16 . (a) $f/N_t=0.01$, (b) $f/N_t=0.1$, (c) $f/N_t=1.0$, and (d) $f/N_t=5.0$.

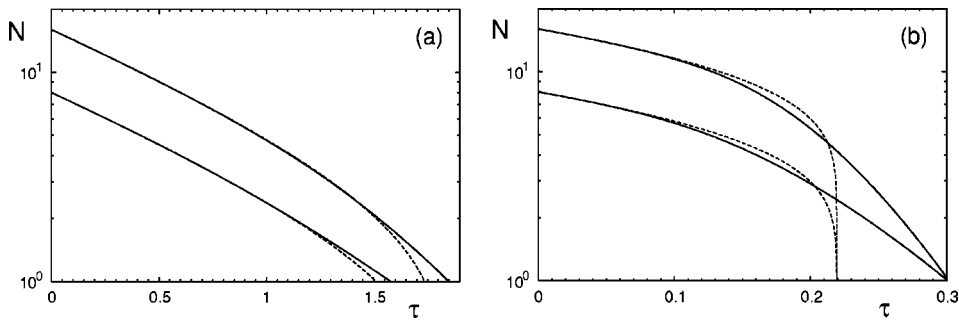


FIG. 4. Average number of closed bonds N as a function of time τ for $N_t=8$ and 16 and (a) $f/N_t=0.1$ and (b) $f/N_t=1$. Solid and dashed lines are stochastic and deterministic results, respectively.

chastic description are compared to each other. For a small but nonzero force, the nonlinearity is small and the agreement between the two results is good in the initial phase of the decay. Towards the end of the decay strong deviations are observed. Here, the force on each bond grows strongly and the nonlinearity of the transition rates is large. For increasing force, fluctuations become less relevant and the deviation between deterministic and stochastic results is increasingly restricted to the very end of the decay process.

In Figs. 5(a) and 5(b) the result for the mean number of closed bonds $N(\tau)$ is compared to single simulation trajectories for small and large forces, respectively. The single simulation trajectories are expected to resemble experimental realizations for the time evolution of the number of closed bonds. The figure shows that for small force, the trajectories decay in a similar way as does the average. For large force, the trajectories decay in a more abrupt way than the averages, that is, they appear to run along the average for most of the time, but then decay rather abruptly towards the completely dissociated state. In this case, fluctuations do not so much affect the typical shape of the rupture trajectory, but rather the timepoint of rupture. The reason for this typical behavior is that a large fluctuation towards the absorbing boundary inevitably leads to a runaway process, since force is increasingly focused on less and less bonds due to shared loading. This type of rupture process is similar to avalanches or cascading failures in highly connected systems. Although rupture is rather abrupt, its timepoint is widely distributed, leading to the smooth decrease of $N(\tau)$ observed in the average. In the large force case in Fig. 5(b), we also show the deterministic results for $N(\tau)$ (for the small force case in Fig. 5(a), they hardly differ from the stochastic results). These curves show that the abrupt decay of single simulation

trajectories at large force is somehow predicted by the deterministic description, compare Fig. 4. This had to be expected because the deterministic equation describes a representative yet single trajectory.

The probability for dissociation of the overall cluster (that is for rupture of the last bond) is defined by $D(\tau) = \dot{p}_0(\tau) = r_1 p_1(\tau)$ and follows from Eq. (23) with the reverse rate r_1 from Eq. (2). The resulting formula has been given before in Ref. 38. For a single bond it is simply $D(\tau) = e^f e^{-e^f \tau}$. For $N_t=2$ we have

$$D(\tau) = \frac{2e^f}{2 - e^{f/2}} (e^{-e^f \tau} - e^{-2e^{f/2} \tau}). \quad (27)$$

In the special case $f = 2 \ln 2$, the two rates $r(1)$ and $r(2)$ are equal and we have

$$D(\tau) = 16\tau e^{-4\tau}. \quad (28)$$

In general, as for $N(\tau)$, $D(\tau)$ is a sum of exponentials $e^{-r(i)\tau}$ and the decrease on long time scales is governed by the exponential which decreases the slowest. In Fig. 6 we plot $D(\tau)$ for different values of N_t and f/N_t (by controlling f/N_t rather than f , the curves have comparable averages). The case $N_t=1$ is a Poisson process with simple exponential decay. For $N_t > 1$, $D(0) = 0$, because instantaneous rupture of all bonds at $\tau=0$ is a higher order process. For large times, all curves decay exponentially. For vanishing force, $f=0$, the curves are very similar, with the same slope at large times. The maxima of the cluster dissociation rates for $f=0$ are described by $T_{\max} = \ln N_t$, in agreement with the result, Eq. (17), from the deterministic description. For small f/N_t , the distributions are Gauss-like with small asymmetry and variance. For large f/N_t , they became Poisson-like, that is, they

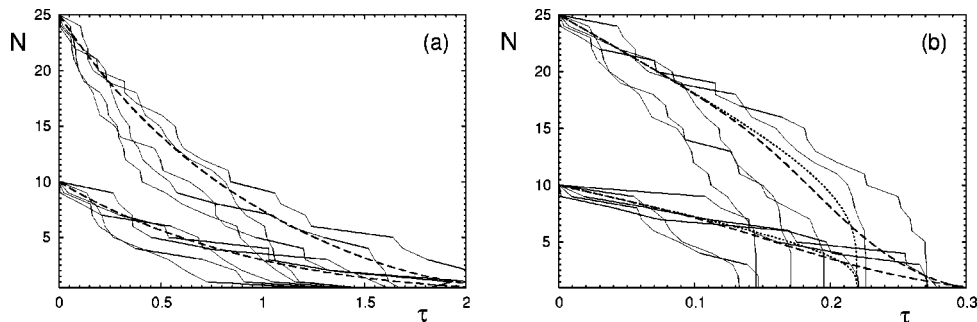


FIG. 5. Single simulation trajectories (solid lines) compared with the average number of closed bonds $N(\tau)$ (dashed lines) for $N_t=10$ and 25 and (a) $f/N_t=0.1$ and (b) $f/N_t=1$. In (b), in addition the deterministic results are plotted as dotted lines.

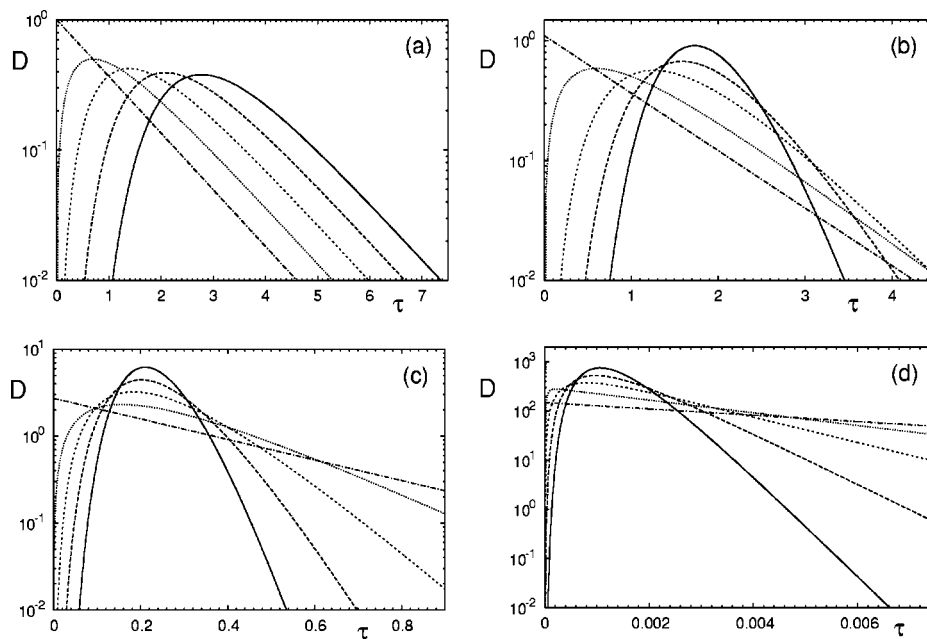


FIG. 6. Probability for dissociation of the whole cluster D as a function of time τ for $N_t = 1, 2, 4, 8,$ and 16 for (a) $f/N_t = 0.0$, (b) 0.1 , (c) 1.0 , and (d) 5.0 .

develop a strong asymmetry with a maximum close to zero and a pronounced long-time tail. The reason is that in this case, decay is dominated by rupture of the first bond, that is, we are effectively back to a single bond system [except that $D(0) = 0$ as always for multiple bonds].

The average cluster lifetime can in principle be calculated as the first moment of the overall dissociation rate

$$T = \int_0^{\infty} d\tau \tau D(\tau). \quad (29)$$

In practice, it has a simple form which can be derived without using the probability distribution Eq. (23). The waiting time spent in state i before the transition into state $i-1$ is a stochastic variable characterized by the distribution function Eq. (21). Its average is given by the inverse transition rate $1/r(i)$. Since the decay process is a sequence of such independent Poisson processes, we simply have

$$T = \sum_{i=1}^{N_t} \frac{1}{r(i)}. \quad (30)$$

For $f=0$ we get^{38,55}

$$T = \sum_{i=1}^{N_t} \frac{1}{i} = H_{N_t}, \quad (31)$$

which are the harmonic numbers. The lifetime of a two-bond cluster is increased by a factor $3/2 = 1.5$ with respect to the single bond, that of the three-bond cluster by $11/6 = 1.8$, and so on. For large N_t one can write⁵⁵

$$T \approx \ln N_t + \frac{1}{2N_t} + \Gamma, \quad (32)$$

where $\Gamma = 0.577$ is the Euler constant. In fact this approximation is very good already for small values of N_t . The weak (logarithmic) dependence for large N_t means that for large adhesion clusters, size matters little since the bonds decay independently of each other and on the same time

scale. This result differs from the deterministic one for small force, Eq. (17), by the constant Γ and the additional contribution $1/2N_t$, which vanishes for large clusters. For small force, $f < 1$, Eq. (32) is a good approximation for cluster lifetime T . For intermediate force, $1 < f < N_t$, the reverse rate grows rapidly for states with $i < f$, whereas for states with $i > f$, $r(i)$ remains close to i . Therefore we can approximate the average lifetime of a cluster as $H_{N_t} - H_f$. Using Eq. (32), we get

$$T \approx \ln(N_t/f). \quad (33)$$

Thus cluster size N_t is now replaced by an effective size N_t/f , as we have already found in the deterministic framework, compare Eq. (19). For large force, $f > N_t$, the only term which contributes to Eq. (30) is the one for the rupture of the first bond. Then

$$T \approx \frac{e^{-f/N_t}}{N_t} \quad (34)$$

and we deal essentially with a single bond effect: if the first bond breaks, all remaining bonds follow within no time (“domino effect”). This effect is also evident from the dissociation rate $D(\tau)$, which for very large force approaches a Poisson distribution, compare Fig. 6(d). In Eq. (34), the numerator represents the probability for single bond rupture under force, while the denominator represents the probability that any one out of N_t identical bonds breaks first. Since $f > N_t$ in this regime, the first effect dominates and T increases with N_t . For a given f/N_t , on the other hand, the lifetime decreases with increasing N_t , due to the increase in absolute force. In contrast to the deterministic result, Eq. (20), the stochastic result Eq. (34) does not scale with f/N_t . In Fig. 7 we plot the average cluster lifetime T from Eq. (30) as a function of f/N_t for different values of N_t . For small force, $f < 1$, T plateaus at the value given by the harmonic number H_{N_t} according to Eq. (31). In the regime of intermediate

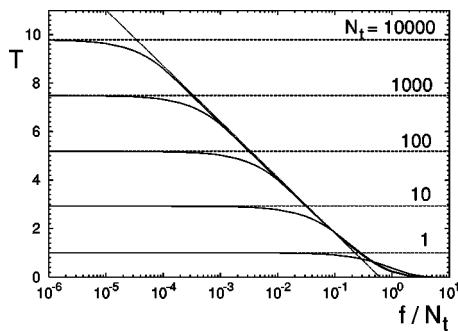


FIG. 7. Average adhesion cluster lifetime T as a function of f/N_t for cluster sizes $N_t=1, 10, 100, 1000,$ and $10\,000$. The dashed horizontal curves are the harmonic numbers, which are good approximations in the small force regime $f < 1$. The dotted curve is the approximation $T = \ln(0.61N_t/f)$ for the intermediate force regime, $1 < f < N_t$.

force, $1 < f < N_t$, all curves fall on the master curve $T = \ln[0.61(N_t/f)]$, as predicted by Eq. (33). For large force, $f > N_t$, the scaling with f/N_t is lost, as predicted by Eq. (34). Although deterministic and stochastic predictions for cluster lifetime T have similar overall features, the deterministic result underestimates the plateau at small force and predicts an incorrect scaling with f/N_t at large force.

Higher cumulants of the various distributions provide information about the effect of fluctuations. For the number of closed bonds at time τ , the width of the distribution is described by the variance, defined by $\sigma_N^2(\tau) = \langle i^2 \rangle - \langle i \rangle^2$. In Fig. 8(a), we plot the relative standard deviation, $\sigma_N(\tau)/N(\tau)$, for cluster sizes $N_t=8$ and $N_t=16$. It is zero initially due to the initial condition and diverges for large times. In regard to the distribution of cluster lifetime, the variance σ_T can be calculated in the same way as the average lifetime, because for a sequence of independent stochastic processes, all cumulants simply add up. The variance of the Poisson process Eq. (21) is $1/r^2(i)$. Therefore the variance for cluster lifetime is

$$\sigma_T^2 = \sum_{i=1}^{N_t} \frac{1}{r^2(i)}. \tag{35}$$

For vanishing force this expression reads

$$\sigma_T^2 = \sum_{i=1}^{N_t} \frac{1}{i^2} = \zeta(2) - \psi^{(1)}(N_t+1), \tag{36}$$

where $\psi^{(1)}(N_t+1)$ is the trigamma function and ζ the Riemannian ζ function. For increasing N_t , the variance converges to a finite value. For zero force this limit is given by

$$\sigma_T^2 = \sum_{i=1}^{\infty} \frac{1}{i^2} = \zeta(2) = \frac{\pi^2}{6}, \tag{37}$$

because the trigamma function vanishes in this limit. This result is an upper limit for the variance in general, because the reverse rate increases with increasing force, $r(i) \geq i$. The relative standard deviation σ_T/T of cluster dissociation is always smaller than unity, since $(\Sigma x)^2 > \Sigma x^2$. For single bond rupture, we have a single Poisson process and it becomes exactly unity. For vanishing force and large clusters, it scales as $\sim 1/\ln N_t$. Although it decreases with increasing N_t , it does so in a different way than the Gauss process, which decreases as $\sim 1/N_t^{1/2}$. The reason is that the contributions from the different subprocesses are not constant, but decrease as rupture proceeds. For large forces, $f > N_t$, cluster dissociation becomes a Poisson process governed by the rupture of the first bond. Then the first term dominates in Eqs. (30) and (35). Therefore the relative standard deviation $\sigma_T/T \approx 1$ again. Moreover, now $\sigma_T/T \sim 1/N_t^{1/2}$, because now only the first $N_t - f$ subprocesses contribute, with roughly similar values, like in a Gauss-distribution. In Fig. 8(b), we plot σ_T/T as a function of f/N_t as it crosses over between the cases of vanishing and very large force, with a minimum around $f/N_t \approx 0.3$, that is, in the intermediate force range. The narrow distribution at intermediate force is also evident in Fig. 6. Figure 8(b) also shows how the relative standard deviation decreases with increasing cluster size N_t . In general, the agreement between deterministic and stochastic descriptions is best for large cluster size N_t and intermediate force $1 < f < N_t$. However, it should also be noted that the definition of deterministic lifetime is somehow arbitrary, because a discrete cutoff has to be introduced in a continuum description. Especially for small clusters the choice of the cluster size at which dissociation occurs will have a large influence on T .

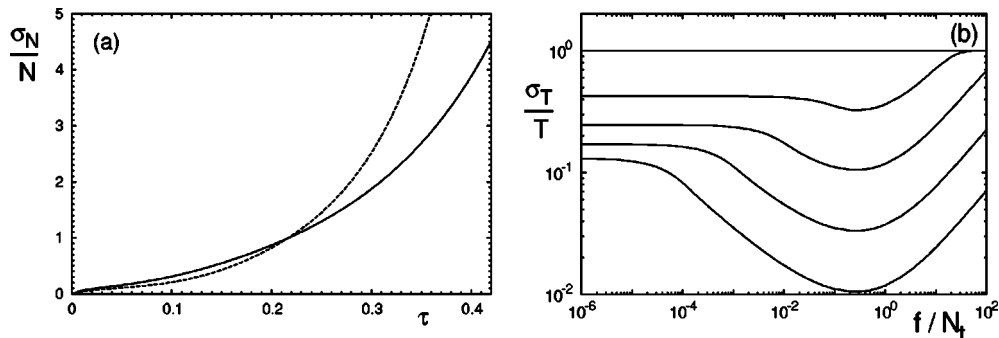


FIG. 8. (a) Variance σ_N for the number of closed bonds in relation to the average number of closed bonds N as function of time τ for $f/N_t=1.0$ and $N_t=8$ (solid) and 16 (dashed). (b) Variance σ_T for cluster lifetime in relation to average cluster lifetime T as a function of f/N_t for $N_t=1, 10, 100, 1000,$ and $10\,000$.

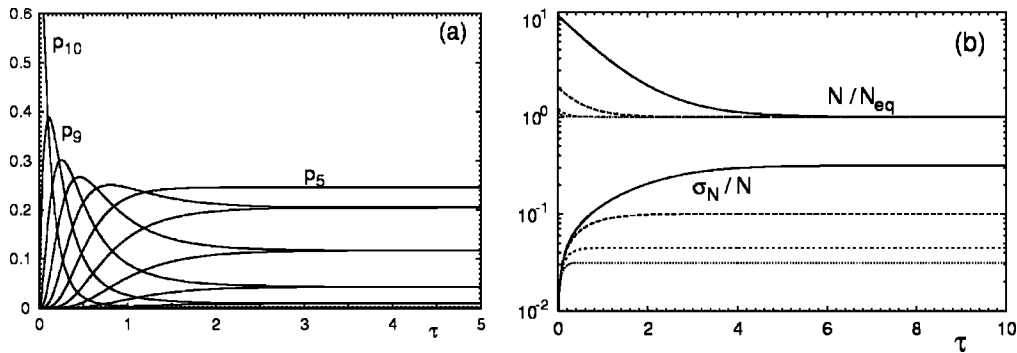


FIG. 9. (a) State probabilities $p_i(\tau)$ from Eq. (41) for $N_t=10$ with $f=0$ and $\gamma=1$ for a reflecting boundary at $i=0$. (b) N/N_{eq} and σ_N/N for $N_t=100$, $f=0$ and $\gamma=0.1, 1, 5$, and 10 .

IV. VANISHING FORCE

A. Deterministic analysis

We now turn to the case of vanishing force, $f=0$. Then the deterministic equation Eq. (4) reads

$$\frac{dN}{d\tau} = -N + \gamma(N_t - N). \quad (38)$$

For the initial condition $N(0)=N_t$, its solution is

$$N(\tau) = \frac{\gamma + e^{-(1+\gamma)\tau}}{1+\gamma} N_t = \left[1 + \frac{1}{\gamma} e^{-(1+\gamma)\tau} \right] N_{eq}. \quad (39)$$

Thus there is an exponentially fast relaxation from N_t to the equilibrium state with $N_{eq} = \gamma N_t / (1 + \gamma)$ closed bonds. N_{eq} increases linearly with the rebinding constant γ from $N_{eq} = 0$ for $\gamma=0$ and saturates at N_t for $\gamma > 1$. In the deterministic description, the lifetime of the cluster is infinite, because the completely dissociated state $N=0$ is never reached.

B. Stochastic analysis

In the case $f=0$, the reverse rates defined in Eq. (2) are linear in i and $r(0)=0$ at $i=0$. Natural boundary conditions imply $g(0) = \gamma N_t$, that is, a reflecting boundary condition at $i=0$. A linear system with natural boundary conditions can be solved with standard techniques. For the initial condition $p_i(0) = \delta_{i,N_t}$, a generating function has been derived by McQuarrie:⁵⁶

$$G(s, \tau) = \sum_{i=0}^{N_t} s^i p_i(\tau) = \left(\frac{(s-1)e^{-(1+\gamma)\tau} + 1 + \gamma s}{(1+\gamma)} \right)^{N_t}. \quad (40)$$

The state probabilities follow from the generating function as

$$p_i(\tau) = \frac{1}{i!} \left. \frac{\partial^i G(s, \tau)}{\partial s^i} \right|_{s=0} = \binom{N_t}{i} \frac{(\gamma + e^{-(1+\gamma)\tau})^i (1 - e^{-(1+\gamma)\tau})^{N_t-i}}{(1+\gamma)^{N_t}}. \quad (41)$$

One can easily check that by setting $\gamma=0$ in Eq. (41), one obtains the same result as by setting $f=0$ in Eq. (23). Equation (41) shows that the system relaxes to the stationary state on a dimensionless time scale $1/(1+\gamma)$, thus the larger

rebinding, the faster the system equilibrates. In the stationary state, the state probabilities follow a binomial distribution

$$p_i(\infty) = \binom{N_t}{i} \frac{\gamma^i}{(1+\gamma)^{N_t}} \quad (42)$$

because the bonds are independent and each bond is closed and open with probabilities $\gamma/(1+\gamma)$ and $1/(1+\gamma)$, respectively.

The generating function also allows to calculate all moments of the distribution:

$$\langle i^n \rangle = \left. \frac{\partial^n G(s, \tau)}{\partial (\ln s)^n} \right|_{s=1}. \quad (43)$$

Since now $r(i)$ is linear in i , the first moment $N(\tau) = \langle i \rangle$ is identical to the solution Eq. (39) of the deterministic equation. In order to assess the role of fluctuations, we calculate the variance:

$$\sigma_N^2(\tau) = \langle i^2 \rangle - \langle i \rangle^2 = \frac{(1 - e^{-(1+\gamma)\tau})}{(1+\gamma)} N(\tau). \quad (44)$$

The relative standard deviation σ_N/N essentially scales as $N^{-1/2}$ for all times, thus fluctuation effects decrease with increasing bond number in the usual way. The stationary state value is $\lim_{\tau \rightarrow \infty} \sigma_N(\tau)/N(\tau) = [(1+\gamma)N_{eq}]^{-1/2} = (\gamma N_t)^{-1/2}$. Therefore larger rebinding does not only increase the equilibrium number of bonds, but also decreases the size of the fluctuations around N_{eq} . This leads to a narrow distribution for large cluster under strong rebinding, with a small probability of coming close to the lower boundary.

In Fig. 9(a), we plot the state probabilities p_i from Eq. (41) for cluster size $N_t=10$ and rebinding constant $\gamma=1$. The system quickly relaxes to the equilibrium state. The only difference for different initial conditions is in the initial transient. In particular, for $N_0=N_{eq}$, the average does not change in time, although the distribution initially spreads to the binomial one. For $\gamma=1$, the stationary distribution is symmetric around the average. The width of the distribution for different γ is illustrated in Fig. 9(b), which shows the average number of closed bonds normalized by the equilibrium number of bonds, that is, N/N_{eq} , together with the relative standard deviation σ_N/N for different values of the rebinding constant γ . The curves for N are independent of N_t

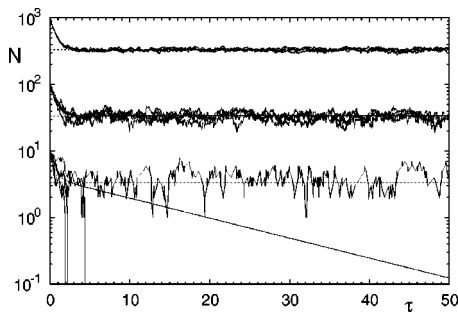


FIG. 10. Single simulation trajectories for $f=0$, $\gamma=0.5$, $N_i=10, 100$, and 1000 and an absorbing boundary at $i=0$. Solid lines are the average number of closed bonds N and dashed lines are the equilibrium number of closed bonds N_{eq} .

due to the normalization. Figure 9(b) shows that with increasing γ , relaxation becomes faster and the width of the distribution decreases.

For the biologically important case of an absorbing boundary at $i=0$, it seems to be rather difficult to find a closed-form analytical solution for arbitrary cluster sizes. For the case $N_i=2$, we will present such a solution in the following section. For arbitrary N_i , we use Monte Carlo simulations as described in Sec. II. In Fig. 10, we show individual simulation trajectories for different parameter values of interest, in comparison to the average number of closed bonds for reflecting and absorbing boundaries at $i=0$. The plots show that the number of closed bonds in a cluster first relaxes towards the steady state value, for which rupture and rebinding balance each other. Although for the absorbing boundary the number of closed bonds decreases with time in average, for individual realizations it stays roughly constant, until a large fluctuation towards the absorbing boundary

leads to loss of this realization. The time scale for the decrease in N is thus determined by the probability for fluctuations from the steady state to the absorbing boundary.

Because a full analytical solution is not available for the case of an absorbing boundary, we now introduce an approximation for this case. It is similar to the local thermal equilibrium description introduced by Zwanzig for modeling protein folding dynamics.⁵⁷ Our starting point is that for large clusters and strong rebinding, the absorbing boundary is a small perturbation to the solution for the reflecting boundary, Eq. (41), which in the following we will denote by $\{\bar{p}_i\}_{i=0}^{N_i}$. Since $g(0)=0$ for the absorbing boundary, $\dot{p}_0 = r_1 p_1$ with $r_1=1$ and probability will only accumulate in the completely dissociated state. Since p_0 is slaved to the other state probabilities and since we expect only a small perturbation for the states with $i \geq 1$, we assume that here the different boundary only leads to a simple renormalization caused by the ‘‘leakage’’ into the absorbing boundary:

$$p_i(\tau) = \bar{p}_i(\tau)[1 - p_0(\tau)] \quad \text{for } i \geq 1, \tag{45}$$

$$p_0(\tau) = \int_0^\tau p_1(\tau') d\tau'.$$

Since relaxation to the steady state is faster than decay to the absorbing boundary, $\bar{p}_i(\tau)$ can be taken to be the stationary value, that is, the constant $\bar{p}_i(\infty)$ according to Eq. (42). Then $p_0(\tau) = \bar{p}_1(\infty) \int_0^\tau [1 - p_0(\tau')] d\tau'$, which is solved by $p_0(\tau) = 1 - e^{-\bar{p}_1(\infty)\tau}$. Therefore Eq. (45) simplifies to

$$p_i(\tau) = \bar{p}_i(\infty) e^{-\bar{p}_1(\infty)\tau} \quad \text{for } i \geq 1, \tag{46}$$

$$p_0(\tau) = 1 - e^{-\bar{p}_1(\infty)\tau}.$$

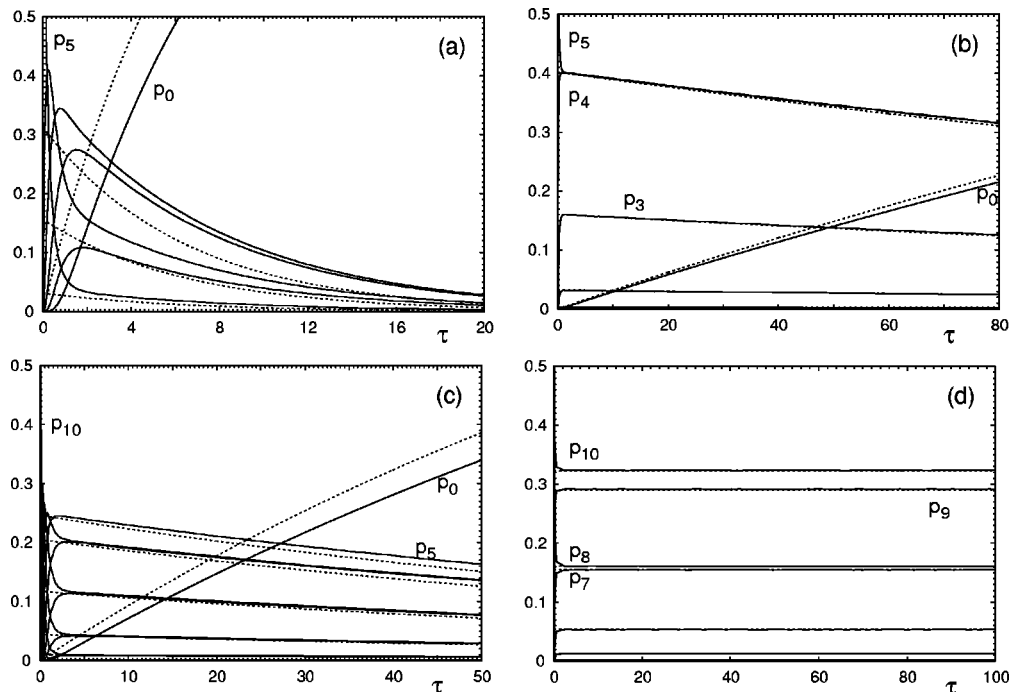


FIG. 11. State probabilities p_i as a function of time τ for different cluster sizes $N_i=5$ (a) and (b) and $N_i=10$ (c) and (d) and for rebinding rates $\gamma=1.0$ (a) and (c) and 5.0 (b) and (d). The numerical solutions (solid curves) are compared to the leakage approximation Eq. (46) (dashed curves).

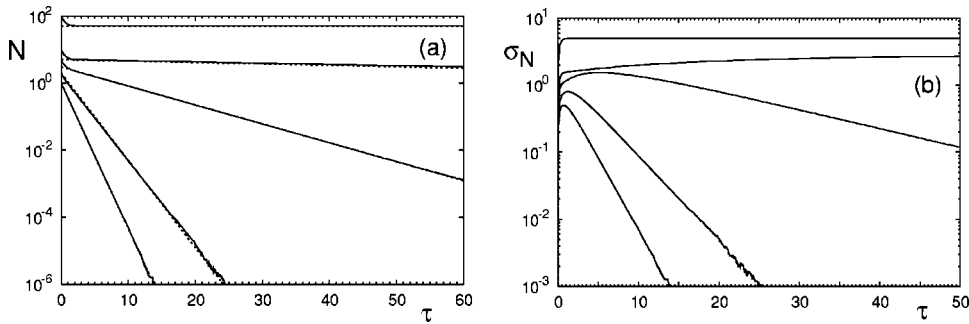


FIG. 12. (a) Average number of closed bonds N obtained from stochastic simulations of the master equation for $\gamma=1$ and $N_t=1, 2, 5, 10$, and 100 . (b) Variance σ_N of the cluster size distribution for the same parameters as in (a).

We conclude that the solution decays exponentially on the time scale $1/\bar{p}_1(\infty)$. In Fig. 11, we plot Monte Carlo solutions for the state probabilities in comparison to the approximation. For $\gamma=1$, the approximation does not work well for $N_t=5$, but it does so already for $N_t=10$. For $\gamma=5$, the approximation works well for both cluster sizes. Note that in this approximation, a term $\bar{p}_0(\infty)e^{-\bar{p}_1(\infty)\tau}$ is missing for proper normalization $\sum_{i=0}^{N_t} p_i=1$. This is a small error for large clusters and strong rebinding. In order to assess the validity of Eq. (46), we note that it presupposes that the time scale for relaxation to the steady state, $1/(1+\gamma)$, is smaller than the time scale for decay to the absorbing boundary, $1/\bar{p}_1(\infty)=(1+\gamma)^{N_t}/\gamma N_t$. Therefore γ should be larger than $(N_{\text{eq}})^{1/N_t}-1$.

It follows from Eq. (46) that the mean number of closed bonds decay in an exponential way, $N(\tau)=N_{\text{eq}}e^{-\bar{p}_1(\infty)\tau}$. This is confirmed by Fig. 12(a), which shows the corresponding simulation results. For $N_t=2, 5$, and 10 , we have $\bar{p}_1(\infty)=0.5, 0.16$, and 9.7×10^{-3} . Numerically we find $0.6, 0.13$, and 0.01 , thus the approximation is rather good. In Fig. 12(b), we plot numerical results for the standard deviation σ_N . The initial increase of σ_N is well described by Eq. (44) for the reflecting boundary, thus the boundary has little influence here. Large clusters stay close to the steady state during the time shown and the approximation is applicable. For small clusters, the variance grows larger than the steady state value before it decreases exponentially while the cluster size N approaches zero. The variance contains two time scales. The second moment of the distribution decreases on the same time scale as the average, while the square of the first moment decreases twice as fast. The long time exponential decrease of σ_N is thus described by twice the relaxation time as is was found for the average number of bonds.

Although an exact solution for the state probabilities seems to be impossible for the case of an absorbing boundary, more analytical progress can be made if one is only interested in the probability that the cluster dissociates as a whole. For the absorbing boundary, the cluster dissociation rate has been denoted by $D(\tau)$ before. For the reflecting boundary, $D(\tau)$ can be identified as the probability that the state $i=0$ is reached for the first time at time τ if the system has started in the state $i=N_t$ at time $\tau=0$. This is a first passage problem which can be treated with Laplace techniques. Since the transition rates do not depend on absolute time, one can decompose the state probability for $i=0$ into two parts:

$$p_0(\tau)=\int_0^\tau D(\tau')p_{0,0}(\tau-\tau')d\tau', \quad (47)$$

where $p_{0,0}(\tau)$ is the state probability for state $i=0$ with initial condition $p_i(0)=\delta_{i,0}$. $p_{0,0}(\tau)$ can also be interpreted as the probability for having returned to the boundary after time τ . A Laplace transform of the equation leads to an algebraic relation between the Laplace transforms of the three functions:

$$D(s)=\frac{p_0(s)}{p_{0,0}(s)}. \quad (48)$$

Here $D(s)=\int_0^\infty e^{-s\tau}D(\tau)$ denotes the Laplace transform of the function $D(\tau)$. The explicit form of the probability $p_0(\tau)$ is given in Eq. (41):

$$p_0(\tau)=\left(\frac{1-e^{-(1+\gamma)\tau}}{1+\gamma}\right)^{N_t}. \quad (49)$$

The probability $p_{0,0}(\tau)$ can also be calculated with standard techniques:⁵⁸

$$p_{0,0}(\tau)=\left(\frac{1+\gamma e^{-(1+\gamma)\tau}}{1+\gamma}\right)^{N_t}. \quad (50)$$

The Laplace transforms of these two functions are given by

$$p_0(s)=\frac{1}{(1+\gamma)^{N_t}}\sum_{i=0}^{N_t}\binom{N_t}{i}\frac{(-1)^i}{s+i(1+\gamma)} \quad (51)$$

and

$$p_{0,0}(s)=\frac{1}{(1+\gamma)^{N_t}}\sum_{i=0}^{N_t}\binom{N_t}{i}\frac{\gamma^i}{s+i(1+\gamma)}, \quad (52)$$

so that the Laplace transformed first passage probability time distribution is

$$D(s)=\frac{\sum_{i=0}^{N_t}\binom{N_t}{i}\frac{(-1)^i}{s+i(1+\gamma)}}{\sum_{i=0}^{N_t}\binom{N_t}{i}\frac{\gamma^i}{s+i(1+\gamma)}}. \quad (53)$$

Unfortunately, the analytical backtransform for $D(s)$ seems to be impossible. However, the mean first passage time can be extracted from this result, because it does not require the backtransform.⁵²

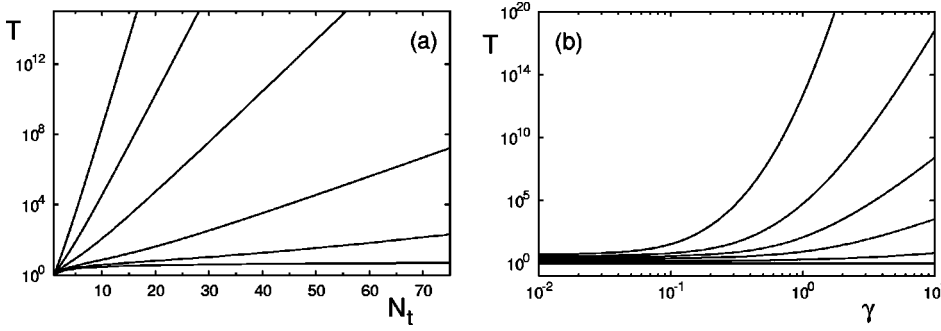


FIG. 13. (a) Average lifetime T of adhesion clusters as function of cluster size N_t for rebinding rates $\gamma=0.0, 0.1, 0.5, 1, 5,$ and 10.0 . (b) Average lifetime T as function of rebinding constant γ for cluster size $N_t=1, 2, 5, 10, 20,$ and 50 .

$$T = \left. \frac{dD(s)}{ds} \right|_{s=0} = \frac{1}{1+\gamma} \left[\sum_{n=1}^{N_t} \left\{ \binom{N_t}{n} \frac{\gamma^n}{n} \right\} + H_{N_t} \right]. \quad (54)$$

This equation is a polynomial of order $N_t - 1$ in γ . The zero order term is the harmonic number H_{N_t} , so for $\gamma=0$ we recover the result from Eq. (31). In Fig. 13, we plot Eq. (54) as a function of cluster size N_t and rebinding rate γ . As long as $\gamma < 1$, cluster lifetime grows only weakly (logarithmically) with cluster size (at least for not too large clusters). For $\gamma > 1$, the higher order terms in γ take over and the increase in T becomes effectively exponential, as shown in Fig. 13(a). In Fig. 13(b), it is shown explicitly that increasing γ to values larger than unity leads to a strong increase in lifetime. This effect is larger for larger clusters since the number of rebinding events in the dissociation path is larger.

V. FINITE FORCE AND FINITE REBINDING

A. Deterministic analysis

Force destabilizes the cluster, while rebinding stabilizes it again. It has been shown by Bell that in the framework, of the deterministic equation, Eq. (4), the cluster remains stable up to a critical force f_c .²³ For the following it is helpful to revisit his stability analysis. In equilibrium we have

$$N_{eq} e^{f/N_{eq}} = \gamma(N_t - N_{eq}). \quad (55)$$

At small force f , this equation has two roots, with the larger one corresponding to a stable equilibrium. As force increases, a saddle-node bifurcation occurs. Above the critical force, no roots exist and the cluster becomes unstable. Exactly at critical loading, the two roots collapse and the slopes of the two terms become equal. This gives an additional equation

$$e^{f_c/N_c} \left(1 - \frac{f_c}{N_c} \right) = -\gamma. \quad (56)$$

These two equations allow to determine the critical values for cluster size and force:

$$f_c = N_t \text{pln} \left(\frac{\gamma}{e} \right) \quad (57a)$$

and

$$N_c = N_t \frac{\text{pln} \left(\frac{\gamma}{e} \right)}{1 + \text{pln} \left(\frac{\gamma}{e} \right)}, \quad (57b)$$

where the product logarithm $\text{pln}(a)$ is defined as the solution x of $xe^x = a$. For small forces, the unstable fixed point is very close to zero. This implies that the stable fixed point is an attractor for most initial conditions. Close to the critical force, the unstable fixed point is close to the stable one and only the initial conditions above N_c will reach the stable fixed point. Equation (57) scales in a trivial way with N_t , but in a complicated way with γ . For $\gamma < 1$, we have $f_c \approx \gamma N_t / e$. Thus the critical force vanishes with γ , because the cluster decays by itself with no rebinding. For $\gamma > 1$ and up to $\gamma \approx 100$, we have $f_c \approx 0.5 N_t \ln \gamma$. This weak dependence on γ shows that the single bond force scale set by F_b also determines the force scale on which the cluster as a whole disintegrates. Figure 14(a) shows how f_c crosses over from linear to logarithmic scaling with γ .

Equation (55) is an implicit equation which cannot be inverted to give N_{eq} as a function of the model parameters N_t, f , and γ . In general, N_{eq} decreases from $\gamma N_t / (1 + \gamma)$ for $f=0$ to N_c for f_c . For small forces we can find an approxi-

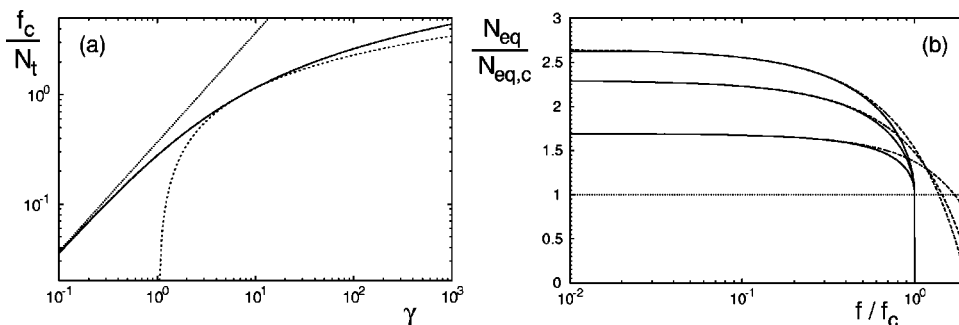


FIG. 14. (a) Critical force Eq. (57) in relation to total cluster size, f_c/N_t , as function of the rebinding constant γ . It scales linearly (dotted curve) at small and logarithmically (dashed curve) for larger γ . (b) Stable steady value for number of closed bonds normalized by the critical value, $N_{eq}/N_{eq,c}$, for $\gamma=0.1, 1,$ and 10 as function of force f/f_c for $N_t=100$. Numerical results (solid lines) are compared to the approximation Eq. (58) (dashed lines). The horizontal line marks the smallest possible value at the critical force f_c .

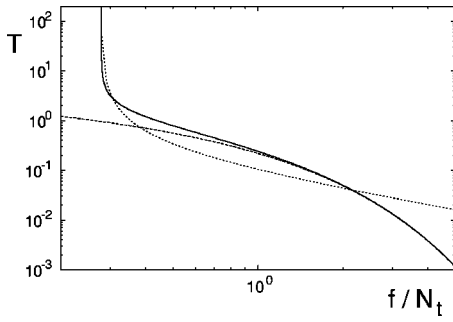


FIG. 15. Deterministic mean lifetime T of a cluster of $N_t=100$ bonds for $\gamma=1$ as a function of the force-size ratio f/N_t . Numerical integration of the deterministic equation (solid line) is compared to the exact solution for vanishing rebinding (dashed line) and the inverse linear scaling (dotted line) predicted close to the critical force.

mate solution by first expanding the exponential function in Eq. (55) to second order in f/N_{eq} and then expanding the resulting quadratic function for N_{eq} to second order in $f/\gamma N_t$:

$$N_{\text{eq}} \approx \frac{\gamma N_t}{1 + \gamma} \left[1 - \left(\frac{f}{\gamma N_t} \right) - \frac{\gamma + 1}{2} \left(\frac{f}{\gamma N_t} \right)^2 \right]. \quad (58)$$

Figure 14(b) shows numerical results for N_{eq}/N_c in comparison with the low force approximation Eq. (58), for different rebinding constants $\gamma=0.1, 1.0$, and 10 as function of force f/f_c and for cluster size $N_t=100$.

In the deterministic framework, cluster lifetime is infinite for $f < f_c$, because a stationary state exists at N_{eq} . For $f > f_c$, cluster lifetime is finite, but strongly varies as a function of N_t , f , and γ . For $f \gg f_c$, we can neglect rebinding and use the results from Sec. III, where we found for cluster lifetime

$$T_{\text{det}} = E \left(\frac{f}{N_t} \right) \approx \frac{e^{-(f/N_t)}}{1 + (f/N_t)}, \quad (59)$$

compare Eq. (20). As force f is decreased from above towards the critical value f_c , rebinding becomes important again and cluster lifetime diverges. To understand this limit, we note that here the system will evolve very slowly, because it is still close to a steady state. Therefore we can expand the time derivative of N , compare Eq. (4), for small deviations from the critical state:

$$\begin{aligned} \frac{dN}{d\tau} &\approx \left. \frac{\partial}{\partial f} \left(\frac{dN}{d\tau} \right) \right|_{f_c, N_c} (f - f_c) \\ &= -e^{f_c/N_c} (f - f_c) = -e^{1 + \text{pln}(\gamma/e)} (f - f_c). \end{aligned} \quad (60)$$

In this limit, the lifetime will be dominated by the time spent close to the critical state. The time for a significant change $\Delta N \approx -1$ in N is

$$T \approx \Delta \tau \approx e^{-[\text{pln}(\gamma/e) + 1]} \frac{1}{f - f_c}. \quad (61)$$

Therefore T diverges like the inverse of $f - f_c$. Figure 15 shows the lifetime of an adhesion cluster derived from numerical integration of the deterministic equation for $\gamma=1$ and $N_t=100$ as a function of the force-size ratio f/N_t . The

numerical results are compared to the approximation, Eq. (59), for large forces and Eq. (61) for the divergence close to the critical point. Obviously both approximations work well for their respective limits. For different cluster sizes N_t , the plot remains basically unchanged (not shown), because the forces above f_c are already in the range where Eq. (16) predicts scaling with f/N_t alone. For different rebinding constants γ the results are qualitatively the same, only that the critical force is shifted to different values.

B. Stochastic analysis

In general, it seems to be difficult to find a closed-form analytical solution for the state probabilities $p_i(\tau)$ for general values of γ , f , and N_t . In the following, we will derive such an analytical solution for the case $N_t=2$ with an absorbing boundary. In principle, solutions can be constructed in the same way for a reflecting boundary or larger clusters, but for increasing cluster size, the analytical procedure quickly becomes intractable. For this reason, we will later use simulations to deal with the general case.

We start by rewriting the master equation, Eq. (1), in matrix form:

$$\dot{\mathbf{p}} = \mathbb{W} \cdot \mathbf{p}. \quad (62)$$

For the case $N_t=2$ with an absorbing boundary, $\mathbf{p} = (p_0, p_1, p_2)^T$ and

$$\mathbb{W} = \begin{pmatrix} 0 & r_1 & 0 \\ 0 & -(r_1 + g_1) & r_2 \\ 0 & g_1 & -r_2 \end{pmatrix}. \quad (63)$$

Equation (62) is solved by⁵²

$$\mathbf{p}(\tau) = e^{\mathbb{W}\tau} \cdot \mathbf{p}(0) = \sum_{\lambda} c_{\lambda} e^{\lambda\tau} \mathbf{p}_{\lambda}, \quad (64)$$

where λ and \mathbf{p}_{λ} are the eigenvalues and eigenvectors of \mathbb{W} , respectively. The coefficients c_{λ} have to be determined from the initial condition

$$\mathbf{p}(0) = \sum_{\lambda} c_{\lambda} \mathbf{p}_{\lambda}. \quad (65)$$

Since the absorbing state $\mathbf{p}_0 = (1, 0, 0)^T$ is a stationary state, the corresponding eigenvalue $\lambda_0 = 0$. The other two eigenvalues are negative and correspond to transient states:

$$\lambda_{1,2} = -(\Omega \pm \omega) \quad (66)$$

with Ω and ω being defined as

$$\Omega = (r_1 + r_2 + g_1)/2 \quad (67a)$$

and

$$\omega = \sqrt{\Omega^2 - r_1 r_2}. \quad (67b)$$

Note that $0 < \omega < \Omega$ and hence $\lambda_{1,2} < 0$. The transient eigenstates are

$$\mathbf{p}_1 = \frac{1}{g_1} \begin{pmatrix} \lambda_2 + r_1 \\ \lambda_1 + r_2 \\ g_1 \end{pmatrix} \quad (68a)$$

and

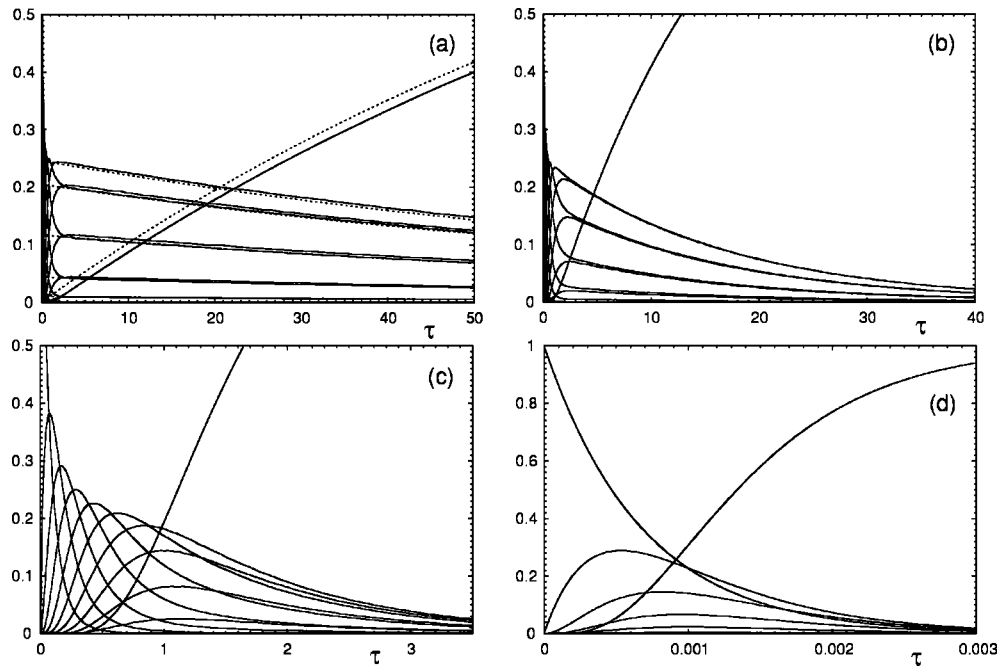


FIG. 16. State probabilities p_i as a function of time τ for $N_i = 10$ with $\gamma = 1$ for force $f = 0.1, 1, 3,$ and 10 (a)–(d). In (a), the numerical solution is compared with the leakage approximation (dotted lines). The intermediate force values are chosen below and above the critical force $f_c = 0.278N_i$.

$$\mathbf{p}_2 = \frac{1}{g_1} \begin{pmatrix} \lambda_1 + r_1 \\ \lambda_2 + r_2 \\ g_1 \end{pmatrix}. \quad (68b)$$

The three eigenstates \mathbf{p}_λ are linearly independent and form a basis of the state space of the cluster. With the initial condition $p_i = \delta_{i,N_i}$, that is, $\mathbf{p}(0) = (0, 0, 1)^T$, the coefficients c_λ follow from Eq. (65) as

$$c_{\lambda_0} = 1, \quad (69a)$$

$$c_{\lambda_1} = \frac{\lambda_2 + r_2}{\lambda_2 - \lambda_1} \quad (69b)$$

and

$$c_{\lambda_2} = -\frac{\lambda_1 + r_2}{\lambda_2 - \lambda_1}. \quad (69c)$$

The final result then can be written as

$$p_0(\tau) = 1 - \left[\cosh(\omega\tau) + \frac{\Omega}{\omega} \sinh(\omega\tau) \right] e^{-\Omega\tau},$$

$$p_1(\tau) = \frac{r_2}{\omega} \sinh(\omega\tau) e^{-\Omega\tau}, \quad (70)$$

$$p_2(\tau) = \left[\cosh(\omega\tau) + \frac{\Omega - r_2}{\omega} \sinh(\omega\tau) \right] e^{-\Omega\tau}.$$

There is a competition between the hyperbolic terms, which grow on the time scale $1/\omega$, and the exponential terms, which decrease on the time scale $1/\Omega$. Since $\omega < \Omega$, the exponential terms will win and only the stationary state survives.

With the exact solution Eq. (70), one now can calculate any quantity of interest. For example, the mean number of bonds, $N(\tau) = \sum_i i p_i$, follows as

$$N(\tau) = \left[2 \cosh(\omega\tau) + \frac{r_1 + g_1}{\omega} \sinh(\omega\tau) \right] e^{-\Omega\tau}. \quad (71)$$

The dissociation rate for the cluster as a whole as given by $D(\tau) = r_1 p_1 = \dot{p}_0$, resulting in

$$D(\tau) = \frac{r_1 r_2}{\omega} \sinh(\omega\tau) e^{-\Omega\tau}. \quad (72)$$

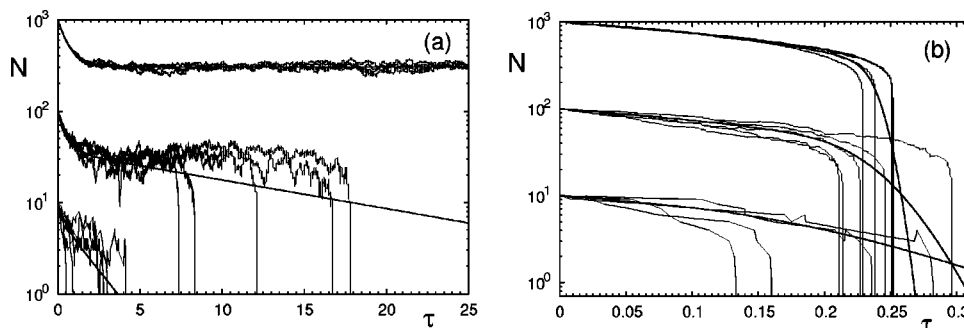


FIG. 17. Single simulation trajectories for $N_i = 10, 100,$ and 100 for $\gamma = 1$ and at two different forces (a) $f = 0.25N_i < f_c$ and (b) $f = N_i > f_c$. Representative trajectories are compared to the average number N of closed bonds resulting from averaging over a large number of such trajectories.

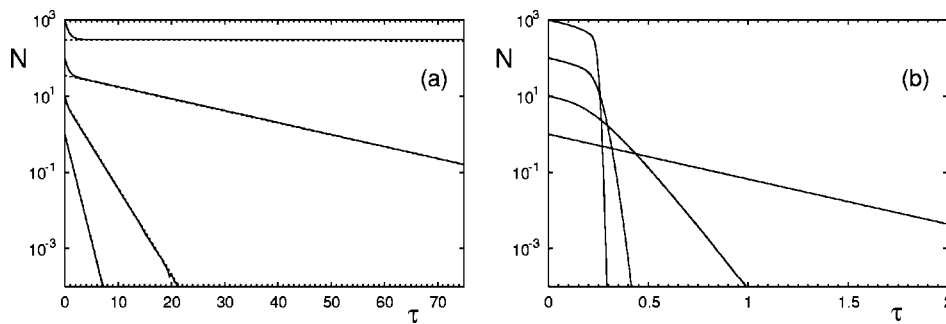


FIG. 18. Average number of closed bonds N for $N_t = 1, 10, 100$, and 1000 , $\gamma = 1$ and (a) $f/N_t = 0.25$ and (b) $f/N_t = 1$. In (a), the numerical results are compared to exponentially decaying curves $\sim e^{-a\tau}$ (dashed lines) with $a = 1.28, 0.52, 0.072$, and 0.0009 for increasing bond number.

One easily checks that normalization is correct, $\int_0^\infty D(\tau) d\tau = 1$. Mean cluster lifetime T now follows as

$$T = \int_0^\infty \tau D(\tau) d\tau = \frac{1}{2} (2e^{-f} + e^{-f/2} + \gamma e^{-3f/2}). \quad (73)$$

As shown in the preceding sections for special cases, force leads to exponentially decreased lifetimes, while rebinding leads to polynomial terms in γ up to order $N_t - 1$.

Although the eigenvalue analysis can be used also for the general case of arbitrary cluster size, in this case it is more efficient to use exact stochastic simulations as described in Sec. II B. In Fig. 16 numerical solutions of the state occupancy probabilities $\{p_i\}_{i=0}^{N_t}$ are plotted for $N_t = 10$ with $\gamma = 1$ for four different forces $f = 0.1, 1, 3$, and 50 . This figure corresponds to Fig. 2 for vanishing rebinding and Fig. 11 for vanishing force. For small force, the numerical solutions compare well with the approximation Eq. (46) introduced for vanishing force. For larger force, but still below the critical force, the state probabilities still decrease exponentially for large times, but the approximation Eq. (46) breaks down, because the reference distribution $\{\bar{p}_i(\infty)\}_{i=0}^{N_t}$ now had to be replaced by the unknown steady state for the case of finite force. If force is increased beyond the critical force ($f_c = 2.78$ for $\gamma = 1$), a simple description is not available, because equilibration and decay occur on the same time scale. For very large force, the behavior of the adhesion cluster approaches that for vanishing rebinding, with the analytical solution, Eq. (23).

Figure 17 demonstrates that the decay process changes dramatically as force is increased above the critical value. It displays trajectories of individual clusters with initially $N_t = N_0 = 10, 100$, and 1000 closed bonds in comparison with the average number of bonds derived from a large number of these trajectories. Since $f_c = 0.278N_t$ for $\gamma = 1$, Fig. 17(a) with $f = 0.25N_t$ is below the critical value. For the largest

cluster, the system equilibrates towards the steady state and then fluctuate around this value with very rare encounters of the absorbing boundary. For the smaller clusters, however, fluctuations towards the absorbing boundary frequently lead to loss of individual realizations. As a result, the average number of closed bonds decays exponentially on a much faster time scale. Figure 17(b) with $f = N_t$ is above the critical force and the behavior is changed qualitatively. A steady state does not exist anymore and the clusters do not decay by fluctuations, but the size of each adhesion cluster is continuously reduced. Clusters of different size now decay on the same time scale and rebinding events are very rare in comparison to rupture events.

Figure 18 plots numerical results for the average number of closed bonds N as function of time τ for two different values of f/N_t and for cluster sizes $N_t = 1, 10, 10^2$, and 10^3 . For $f = 0.25N_t < f_c$, after initial relaxation all curves decay exponentially. For $f = N_t > f_c$, the larger clusters show a steep decrease in average cluster size at the end of the decay due to the effects of shared loading. For the small clusters, the average cluster size decreases slowly since cooperative effects are small.

Figure 19 plots the variance $\sigma_N(\tau)$ of the distribution p_i for the two force values used in the two previous figures. Below the critical force the behavior is similar to that for vanishing force depicted in Fig. 12. The variance decreases exponentially after having traversed a maximum. For forces above the critical force, a different behavior arises. After growing as expected in the initial phase, the variance displays a sharp peak. This effect becomes more pronounced with larger cluster size.

In Fig. 20 a comparison of the average number of closed bonds in the stochastic and the deterministic description is shown. $N(\tau)$ is plotted for cluster sizes $N_t = 10, 100$, and 1000 for the forces $f/N_t = 0.1$ and 1.0 and the rebinding rate

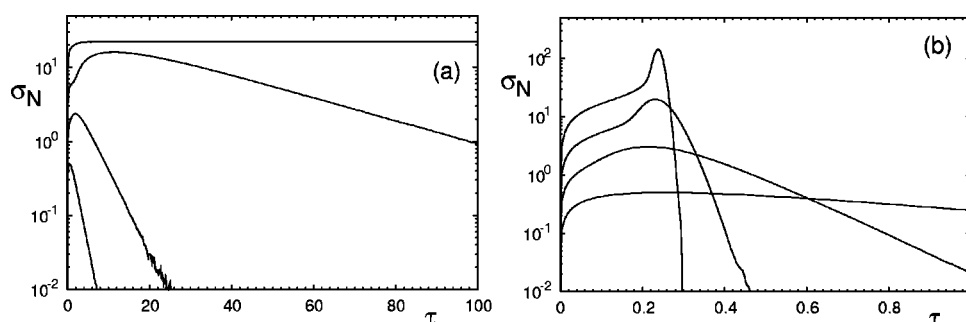


FIG. 19. Variance σ_N for forces (a) $f = 0.25N_t$ and (b) $f = N_t$ for $\gamma = 1$ and $N_t = 1, 10, 100$, and 1000 .

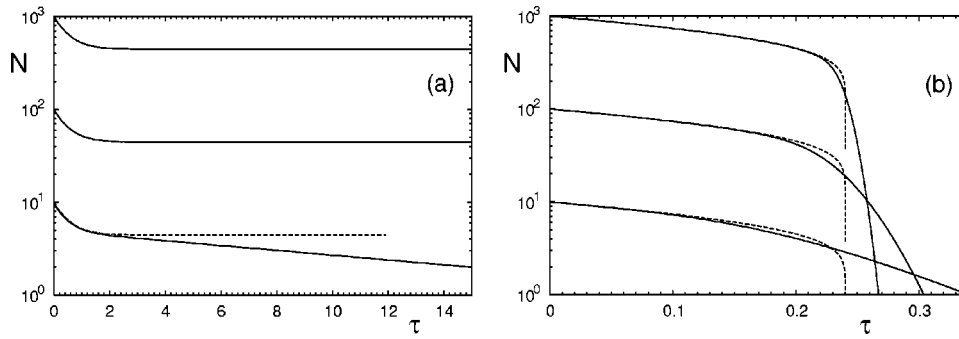


FIG. 20. Comparison of stochastic and deterministic results for the average number of closed bonds N derived from numerical solutions of the master equation (solid lines) and from integration of the deterministic equation (dashed curves) for cluster sizes $N_t = 10, 100,$ and 1000 and forces (a) $f/N_t = 0.1$ and (b) 1.0 . The rebinding rate is $\gamma = 1$.

$\gamma = 1.0$. For small forces $f < f_c$, the average number of closed bonds equilibrates towards the steady state and remains constant thereafter. The fluctuations occurring in the stochastic description lead to a slow decrease of N . Above the critical force, the deterministic clusters decay as well, and in a more abrupt way than the stochastic average.

We now turn to the dissociation rate of the overall cluster as a function of the model parameters. For $\gamma = 1$ and $f = 0.25N_t$ and N_t , that is, below and above the critical force, numerical results are plotted in Fig. 21. For a single bond, dissociation is a Poisson process with the maximum at $\tau = 0$ and an exponentially decreasing dissociation rate $D = r(1)p_1 = e^f e^{-e^f \tau}$. For larger clusters and below the critical force, fluctuations to the absorbing boundary determine the rate of dissociation, which vanishes at $\tau = 0$, goes through a maximum and then decreases exponentially with time. As explained above, the exponential decay follows because decay proceeds by rare fluctuations from the steady state towards the absorbing boundary. Above the critical force, the dissociation rate for $N_t > 1$ becomes more sharply peaked and cannot be described with single exponential curves. A steady state does not exist anymore and dissociation does not proceed by fluctuations. The trajectories in Fig. 17 have shown that adhesion clusters decay fairly abrupt towards the end of the decay as a consequence of shared loading. This cooperative instability is the reason for the sharp dissociation distribution for large clusters under supercritical loading. The single bond that lacks this cooperativity still shows the exponential dissociation rate, which is now the slowest decaying for the given force-size ratio.

Whereas results for the dissociation rate have to be obtained numerically, the average lifetime can be calculated analytically.⁵¹ The basic idea here is to sum the average times for any possible pathway leading from the initial cluster size N_0 towards dissociation at the absorbing boundary

$i = 0$ with its appropriate statistical weight. One can show that the lifetime T_{N_t, N_0} of a cluster with a total of N_t molecular bonds of which N_0 are closed initially satisfies the equation⁵¹

$$g(N_0)(T_{N_t, N_0+1} - T_{N_t, N_0}) + r(N_0)(T_{N_t, N_0-1} - T_{N_t, N_0}) = -1. \quad (74)$$

The left hand side can be considered to be the adjoint operator of the master equation acting on the average lifetime T_{N_t, N_0} . For the initial condition $N_0 = N_t$, the equation is solved exactly by

$$T = T_{N_t, N_t} = \sum_{i=1}^{N_t} \frac{1}{r(i)} + \sum_{i=1}^{N_t-1} \sum_{j=i+1}^{N_t} \frac{\prod_{k=j-i}^{j-1} g(k)}{\prod_{k=j-i}^j r(k)}, \quad (75)$$

where the first term is the result, Eq. (30), for vanishing rebinding and the second term results in a polynomial of order $N_t - 1$ in γ . For $f = 0$, Eq. (75) is identical to the earlier result Eq. (54) obtained by Laplace transforms. Both expressions are polynomials of order $N_t - 1$ in γ , but in the general case from Eq. (75), the coefficients depend on force. For $N_t = 2$, we obtain the result from Eq. (73). For $N_t = 3$, we find

$$T = e^{-f} + \frac{e^{-f/2}}{2} + \frac{e^{-f/3}}{3} + \gamma \left(\frac{e^{-5f/6}}{6} + e^{-3f/2} \right) + \gamma^2 \frac{e^{-11f/6}}{3}. \quad (76)$$

For $N_t = 2$ and 3 , T can also be derived by explicitly summing over all possible dissociation paths. For larger N_t , direct summation becomes intractable and the results following from the general formula Eq. (75) become rather lengthy. In general, force always affects most strongly those terms of highest order in γ , thus for $\gamma > 1$, application of force is therefore an efficient way to reduce average lifetime T . For

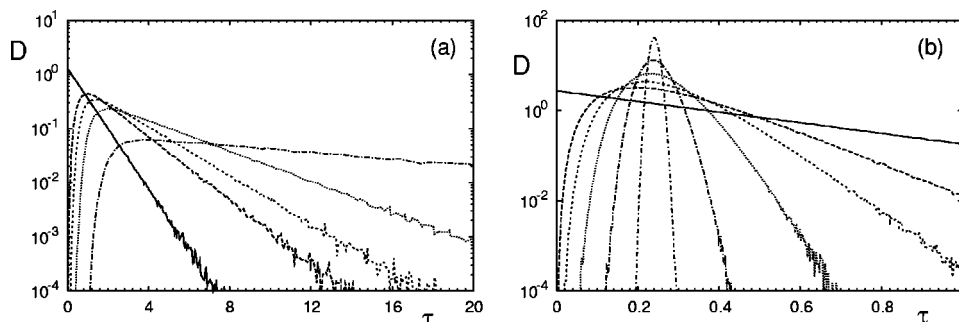


FIG. 21. Dissociation rate D of the overall cluster for $\gamma = 1$ and $N_t = 1, 5, 10, 25, 100,$ and 1000 . (a) $f = 0.25N_t$ and (b) $f = N_t$.

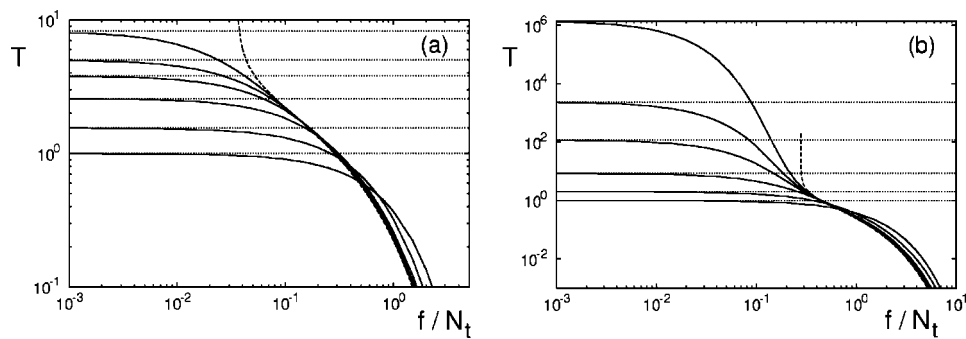


FIG. 22. Average lifetime T according to Eq. (75) (solid lines) of adhesion clusters with $N_t=1, 2, 5, 10, 15,$ and 25 as a function of f/N_t for (a) $\gamma=0.1$ and (b) $\gamma=1$. The critical forces for these rebinding rates are $f_c/N_t=0.0355$ and 0.278 , respectively, where the deterministic results for the lifetimes (dashed lines) diverge.

$\gamma < 1$, T is dominated by those terms of lowest order in γ , thus here the reduction of lifetime with increasing force is not modulated by rebinding.

Figure 22 shows the average lifetime of adhesion clusters of size $N_0=1, 2, 5, 10, 15,$ and 25 as a function of force-size ratio f/N_t for the rebinding constants $\gamma=0.1$ and $\gamma=1.0$. For small forces, $f < 1$, the average lifetime plateaus at the value given by Eq. (54). For large forces, $f > N_t$, that is, when the force on each single bond is larger than the intrinsic force scale, the limit of vanishing rebinding applies (for $N_t=1$ lifetime is independent of γ , compare also Fig. 15). The critical forces for the given rebinding rates are $f_c=0.0355N_t$ and $f_c=0.278N_t$. In the intermediate force range, roughly around f_c , the lifetime is reduced from the zero force to the zero rebinding limit. This reduction is dramatic for large clusters ($N_t \geq 10$) with appreciable rebinding ($\gamma \geq 1$), where the lifetime is reduced by orders of magnitude. We also show the lifetime following from the deterministic framework, which provides a lower limit for the lifetime at large forces, because here the largest clusters have the shortest lifetimes for a given force-size ratio f/N_t . Below the critical force the deterministic lifetime is infinite and the stochastic curves approach the plateaus, Eq. (54), determined by fluctuations towards the absorbing boundary.

Figure 23(a) demonstrates the influence of rebinding on the average lifetime at different levels of force. Here we show average lifetime T as function of γ for $N_t=10$ and for increasing values of force. For $f=0$ the curves are as depicted in Fig. 13. Increasing force reduces the lifetime strongly and leads to an almost constant lifetime for different γ (compared to the strong increase for $f=0$). Only when rebinding is sufficiently strong that force is smaller than the critical force, $f < f_c$, lifetime begins to grow. The increase observed then is similar to that for vanishing force, only that

the absolute value of lifetime is smaller. For example, for $f=0.6N_t$, the cluster grows strongly for $g \geq 5$ where the critical force is $f_c=0.82N_t$; for $f=N_t$ the strong increase is observed for $g \geq 10$, for which the critical force is $f_c=1.15N_t$. A similar effect is observed for the dependence of average lifetime on cluster size, see Fig. 23(b). At small N_t , cluster lifetime grows strongly at large forces according to Eq. (30) due to shared loading. For larger N_t , lifetime grows slowly until N_t is large enough that $f_c \geq f$ is reached. Above this size, T grows on a rate comparable to that for vanishing or small force. For $\gamma=0.1$, the increase of T with N_t is slow throughout the shown range of N_t .

VI. DISCUSSION

In this paper, we have presented a detailed analysis of the stochastic dynamics of an adhesion cluster of size N_t under shared loading f and with rebinding rate γ . The corresponding master equation has been solved exactly for several special cases. For vanishing rebinding ($\gamma=0$), the exact solution Eq. (23) could be constructed because cluster decay is a sequence of Poisson processes. For vanishing force ($f=0$), we deal with a linear problem, which can be treated with standard techniques. In the case of natural boundaries (that is for a reflecting boundary at $i=0$), the exact solution Eq. (41) follows with the help of a generating function. In the general case of finite force f and finite rebinding rate γ , for the case $N_t=2$ and an absorbing boundary we used an eigenvalue analysis to derive the exact solution Eq. (70). In principle, the same method can also be applied for a reflecting boundary or for larger clusters, but this does not lead to simple analytical results.

For vanishing force ($f=0$) and an absorbing boundary at $i=0$, we introduced the ‘leakage approximation’ (also

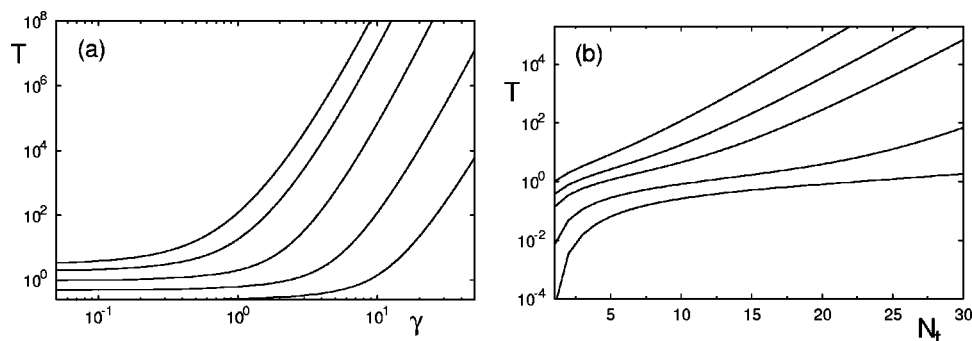


FIG. 23. Average cluster lifetime T (a) as function of rebinding rate γ for $N_t=10$ and $f/N_t=0, 0.1, 0.3, 0.6,$ and 1 and (b) as function of cluster size N_t for $\gamma=1.0$ and $f=0, 1, 2,$ and 10 .

known as “local thermal equilibrium description” in the theory of protein folding), which treats the absorbing boundary as a small perturbation to the exactly solved case of the reflecting boundary. The resulting formulas given in Eq. (46) work well if average cluster lifetime T is much larger than the internal time scale $1/(1 + \gamma)$ (that is for large clusters or strong rebinding). All other cases have been treated with exact stochastic simulations using the Gillespie algorithm, which for large clusters is more efficient than the eigenvalue analysis. Moreover, the study of single simulation trajectories offers valuable insight into the typical nature of unbinding trajectories expected for experiments.

Once the master equation is solved, either exactly or numerically, all quantities of interest can be calculated. In this paper, we focused on the mean number of closed bonds as a function of time $N(\tau)$, and the dissociation rate for the overall cluster $D(\tau)$. The first moment of $D(\tau)$ then gives the mean cluster lifetime T . In this paper, we derived an exact solution $T = T(N_t, f, \gamma)$ from the adjoint master equation, see Eq. (75). For the special cases of vanishing rebinding and vanishing force, we also showed how the exact formulas for T can be derived via completely different routes. The result for $T = T(N_t, f)$ from Eq. (30) follows from the unique dissociation path without rebinding, while the result for $T = T(N_t, \gamma)$ from Eq. (54) can be derived with Laplace techniques as a mean first passage time for the case of a reflecting boundary. In order to assess the role of fluctuations, we also calculated the standard deviations σ_N and σ_T for the distributions of the number of closed bonds and cluster lifetimes, respectively.

A special focus of this paper was a detailed comparison between the stochastic and deterministic treatment. Regarding mean cluster lifetime, the deterministic treatment is rather good in the case of vanishing rebinding, although it underestimates the plateau value for cluster lifetime at small force. In the presence of rebinding, the deterministic treatment fails, because it includes neither the effect of fluctuations nor the effect of an absorbing boundary. In particular, the deterministic treatment does not predict finite lifetime below the critical force f_c , when clusters decay due to fluctuations towards the absorbing boundary. Only at very large force, when rebinding becomes irrelevant, does the deterministic treatment work well again. Regarding the average number of closed bonds, the deterministic model fails because it does not correctly treat the nonlinearity in the rupture rate. This effect is most evident for small clusters and at late stage of rupture. In general, the mean number of closed bonds in the stochastic model decay in a smoother way than in the deterministic model, which typically shows an abrupt decay in late stage. This abrupt decay in fact is typical for shared loading and shows up in the stochastic model when one studies single simulation trajectories. In this sense, the deterministic model makes an interesting prediction which should be confirmed in experiment, albeit not on the level of the first moment, as suggested by the deterministic model, but rather on the level of single trajectories, as suggested by the stochastic model.

Our results can now be used to evaluate a large range of different experimental situations. The stochastic dynamics of

adhesion clusters under force can be quantitatively studied with many different techniques, including atomic force microscopy, optical tweezers, magnetic tweezers, the biomembrane force probe, flow chambers, and the surface force apparatus. In all of these cases, by measuring cluster lifetime T and two out of the three parameters N_t , f , and γ , the third parameter can be estimated with the help of our exact results. In general, our exact results nicely show how mean cluster lifetime T varies with cluster size N_t , force f and rebinding rate γ . For example, if the single bond lifetime was one second ($k_0 = 1/s$), for $f = 0$ and $\gamma = 0$ a cluster lifetime T of one minute could only be achieved with 10^{26} bonds, because in this case, cluster lifetime scales only logarithmically with cluster size. However, for a rebinding rate $\gamma = 1$ ($k_{on} = k_0$), only $N_t = 10$ bonds are necessary, because lifetime scales strongly with rebinding, $T \sim \gamma^{N_t - 1}$. Increasing force to $f = 10$ would decrease lifetime to $T = 0.05$ s, because T is exponentially decreased by f . To reach one minute again, cluster size or rebinding rate had to be increased such that $f < f_c$. This implies $N_t > 50$ or $\gamma > 10$. It is important to note that these predictions are based on the assumption of rigid force transducers. In many experimental situations of interest, the force transducer will be subject to elastic deformations or even to viscous relaxation processes, like for example when pulling on cells.⁵⁹ In order to focus on generic aspects of adhesion clusters, here we only studied the minimal model for stochastic dynamics under force.

Our results can also be applied to experiments in cell adhesion. For example, the biomembrane force probe with linear loading has recently been used to study the decay of $\alpha_v\beta_3$ -integrin clusters induced on the surface of endothelial cells.^{29,41} If one makes sure that the clusters do not actively grow during the time of dissociation, similar experiments could now be done also for constant loading. Because in these kinds of experiments the exact cluster size is usually unknown, one had to convolute our results with a Poisson distribution for an estimated average number of bonds.^{34,39} Recently, our result for the average cluster lifetime of two bonds under shared force and with rebinding, Eq. (73), has been applied to the analysis of flow chamber data on leukocyte tethering through L-selectin.⁴² Since in this case force can be calculated as a function of shear flow, our formula can be used to estimate rebinding rate, which in this case turns out to be surprisingly large. This in turn explains why dissociation dynamics in L-selectin mediated leukocyte tethering appears to be first order: for large rebinding, the leakage approximation is rather good, and decay is exponential.

Our results cannot be directly applied to adhesion clusters which compensate for force-induced decay by active growth, as it has been found experimentally for focal adhesions.⁶⁰ Yet there are also interesting lessons for focal adhesions which can be learned from our model. For example, our stochastic analysis confirms the prediction from the deterministic stability analysis that cluster stability changes strongly around the critical value f_c (although small clusters tend to decay also at smaller force due to fluctuations towards the absorbing boundary). It is interesting to note that recent experiments measuring internally generated force at single focal adhesions suggest that f/N_t , the most

important scaling variable of our analysis, is roughly constant for different cell types.^{43,45} It is therefore tempting to speculate that focal adhesions (or subsets of focal adhesions) are regulated to be loaded close to the critical value $f_c/N_t = \text{pln}(\gamma/e)$ from Eq. (57). In this way, cells could quickly increase force on single bonds by small changes in actomyosin contractility. Large force on single closed bonds in turn might trigger certain signaling events in focal adhesions, possibly by mechanically opening up certain signaling domains.⁶¹ Our speculation provides a simple way to estimate the rebinding rate, which is very hard to measure experimentally. Using compliant substrates, it has been found that focal adhesions are characterized by a stress constant $\sim 5.5 \text{ nN}/\mu\text{m}^2$.^{43,45} We do not know which of the many different proteins in focal adhesions defines the weak link which most likely ruptures under force, but we expect that it will have a similar area density as the integrin receptors, which are expected to have a typical distance between 10 and 30 nm, corresponding to 10^4 and 10^3 molecules per μm^2 , respectively. To obtain a lower estimate for γ , we therefore use $F_c = 5.5 \text{ nN}$ and $N_t = 10^4$. For activated $\alpha_5\beta_1$ -integrin binding to fibronectin, recent single molecule experiments obtained for the molecular parameter values $k_0 = 0.012 \text{ Hz}$ and $F_b = 9 \text{ pN}$.¹⁹ Therefore the rebinding rate can be estimated to be at least $\gamma = 0.2$, that is, $k_{\text{on}} = 0.002 \text{ Hz}$ in dimensional units. Based on future experimental input, it would be interesting to extend our model of passive decay to active processes resulting in cluster growth under force.

Finally we want to comment that our model might also be applied to situations in materials science which are not directly related to biomolecular receptor-ligand pairs. One example is sliding friction, which recently has been modeled as dynamic formation and rupture of bonds under force.⁶² In general, we expect that many more cohesion phenomena in materials can be successfully modeled as dynamic interplay between rupture and rebinding.

ACKNOWLEDGMENT

This work was supported by the German Science Foundation through the Emmy Noether Program.

- ¹B. Alberts, A. Johnson, J. Lewis, M. Raff, K. Roberts, and P. Walter, *Molecular Biology of the Cell*, 4th ed. (Garland Science, New York, 2002).
- ²E. Evans, *Annu. Rev. Biophys. Biomol. Struct.* **30**, 105 (2001).
- ³R. Merkel, *Phys. Rep.* **346**, 344 (2001).
- ⁴J. W. Weisel, H. Shuman, and R. I. Litvinov, *Curr. Opin. Struct. Biol.* **13**, 227 (2003).
- ⁵E.-L. Florin, V. T. Moy, and H. E. Gaub, *Science* **264**, 415 (1994).
- ⁶E. Evans and K. Ritchie, *Biophys. J.* **72**, 1541 (1997).
- ⁷M. Rief, M. Gautel, F. Oesterhelt, J. M. Fernandez, and H. E. Gaub, *Science* **276**, 1109 (1997).
- ⁸M. S. Z. Kellermayer, S. B. Smith, H. L. Granzier, and C. Bustamante, *Science* **276**, 1112 (1997).
- ⁹R. Merkel, P. Nassoy, A. Leung, K. Ritchie, and E. Evans, *Nature (London)* **397**, 50 (1999).
- ¹⁰D. A. Simson, M. Strigl, M. Hohenadl, and R. Merkel, *Phys. Rev. Lett.* **83**, 652 (1999).
- ¹¹R. Alon, D. A. Hammer, and T. A. Springer, *Nature (London)* **374**, 539 (1995).
- ¹²A. Pierres, D. Touchard, A.-M. Benoliel, and P. Bongrand, *Biophys. J.* **82**, 3214 (2002).
- ¹³D. A. Lauffenburger and J. J. Linderman, *Receptors: Models for Binding,*

- Trafficking, and Signalling* (Oxford University Press, Oxford, 1993).
- ¹⁴S. Izrailev, S. Stepaniants, M. Balsera, Y. Oono, and K. Schulten, *Biophys. J.* **72**, 1568 (1997).
 - ¹⁵J. Shillcock and U. Seifert, *Phys. Rev. E* **57**, 7301 (1998).
 - ¹⁶B. Heymann and H. Grubmüller, *Phys. Rev. Lett.* **84**, 6126 (2000).
 - ¹⁷O. Braun, A. Hanke, and U. Seifert, *cond-mat/0402496*.
 - ¹⁸X. Zhang, E. Wojcikiewicz, and V. T. Moy, *Biophys. J.* **83**, 2270 (2002).
 - ¹⁹F. Li, S. D. Redick, H. P. Erickson, and V. T. Moy, *Biophys. J.* **84**, 1252 (2003).
 - ²⁰W. Baumgartner, P. Hinterdorfer, W. Ness, A. Raab, D. Vestweber, H. Schindler, and D. Drenckhahn, *Proc. Natl. Acad. Sci. U.S.A.* **97**, 4005 (2000).
 - ²¹J. Fritz, A. G. Katopodis, F. Kolbinger, and D. Anselmetti, *Proc. Natl. Acad. Sci. U.S.A.* **95**, 12283 (1998).
 - ²²E. Evans, A. Leung, D. Hammer, and S. Simon, *Proc. Natl. Acad. Sci. U.S.A.* **98**, 3784 (2001).
 - ²³G. I. Bell, *Science* **200**, 618 (1978).
 - ²⁴M. Dembo, D. C. Torney, K. Saxman, and D. Hammer, *Proc. R. Soc. London, Ser. B* **234**, 55 (1988).
 - ²⁵D. A. Hammer and S. M. Apte, *Biophys. J.* **63**, 35 (1992).
 - ²⁶K.-C. Chang, D. F. J. Tees, and D. A. Hammer, *Proc. Natl. Acad. Sci. U.S.A.* **97**, 11262 (2000).
 - ²⁷U. Seifert, *Phys. Rev. Lett.* **84**, 2750 (2000).
 - ²⁸U. Seifert, *Europhys. Lett.* **58**, 792 (2002).
 - ²⁹K. Prechtel, A. R. Bausch, V. Marchi-Artzner, M. Kantschler, H. Kessler, and R. Merkel, *Phys. Rev. Lett.* **89**, 028101 (2002).
 - ³⁰D. Zuckermann and R. Bruinsma, *Phys. Rev. Lett.* **74**, 3900 (1995).
 - ³¹R. Lipowsky, *Phys. Rev. Lett.* **77**, 1652 (1996).
 - ³²T. R. Weikl and R. Lipowsky, *Phys. Rev. E* **64**, 011903 (2001).
 - ³³A. Albersdorfer, T. Feder, and E. Sackmann, *Biophys. J.* **73**, 245 (1997).
 - ³⁴S. E. Chesla, P. Selvaraj, and C. Zhu, *Biophys. J.* **75**, 1553 (1998).
 - ³⁵R. Bruinsma, A. Behrisch, and E. Sackmann, *Phys. Rev. E* **61**, 4253 (2000).
 - ³⁶D. A. Hammer and D. A. Lauffenburger, *Biophys. J.* **52**, 475 (1987).
 - ³⁷C. Cozens-Roberts, D. A. Lauffenburger, and J. A. Quinn, *Biophys. J.* **58**, 841 (1990).
 - ³⁸D. F. J. Tees, J. T. Woodward, and D. A. Hammer, *J. Chem. Phys.* **114**, 7483 (2001).
 - ³⁹C. Zhu, *J. Biomech.* **33**, 23 (2000).
 - ⁴⁰T. Erdmann and U. S. Schwarz, *Phys. Rev. Lett.* **92**, 108102 (2004).
 - ⁴¹T. Erdmann and U. S. Schwarz, *Europhys. Lett.* **66**, 603 (2004).
 - ⁴²U. S. Schwarz and R. Alon, *Proc. Natl. Acad. Sci. U.S.A.* **101**, 6940 (2004).
 - ⁴³N. Q. Balaban, U. S. Schwarz, D. Riveline *et al.*, *Nat. Cell Biol.* **3**, 466 (2001).
 - ⁴⁴U. S. Schwarz, N. Q. Balaban, D. Riveline, A. Bershadsky, B. Geiger, and S. A. Safran, *Biophys. J.* **83**, 1380 (2002).
 - ⁴⁵J. L. Tan, J. Tien, D. M. Pirone, D. S. Gray, K. Bhadriraju, and C. S. Chen, *Proc. Natl. Acad. Sci. U.S.A.* **100**, 1484 (2003).
 - ⁴⁶R. Alon, S. Chen, K. D. Puri, E. B. Finger, and T. A. Springer, *J. Cell Biol.* **138**, 1169 (1997).
 - ⁴⁷C. E. Orsello, D. A. Lauffenburger, and D. A. Hammer, *Trends Biotechnol.* **19**, 310 (2001).
 - ⁴⁸C. Jeppesen, J. Y. Wong, T. L. Kuhl, J. N. Israelachvili, N. Mullah, S. Zalipsky, and C. M. Marques, *Science* **293**, 465 (2001).
 - ⁴⁹A. G. Moreira, C. Jeppesen, F. Tanaka, and C. M. Marques, *Europhys. Lett.* **62**, 876 (2003).
 - ⁵⁰A. G. Moreira and C. M. Marques, *J. Chem. Phys.* **120**, 6229 (2004).
 - ⁵¹N. G. van Kampen, *Stochastic Processes in Physics and Chemistry* (Elsevier, Amsterdam, 1992).
 - ⁵²J. Honerkamp, *Stochastische Dynamische Systeme* (VCH, Weinheim, 1990).
 - ⁵³D. T. Gillespie, *J. Comput. Phys.* **22**, 403 (1976).
 - ⁵⁴D. T. Gillespie, *J. Phys. Chem.* **81**, 2340 (1977).
 - ⁵⁵B. Goldstein and C. Wofsy, *Immunol. Today* **17**, 77 (1996).
 - ⁵⁶D. A. McQuarrie, *J. Chem. Phys.* **38**, 433 (1963).
 - ⁵⁷R. Zwanzig, *Proc. Natl. Acad. Sci. U.S.A.* **92**, 9801 (1995).
 - ⁵⁸N. S. Goel and N. Richter-Dyn, *Stochastic Models in Biology* (Academic, New York, 1974).

⁵⁹M. Benoit, D. Gabriel, G. Gerisch, and H. E. Gaub, *Nat. Cell Biol.* **2**, 313 (2000).
⁶⁰D. Riveline, E. Zamir, N. Q. Balaban, U. S. Schwarz, B. Geiger, Z. Kam, and A. D. Bershadsky, *J. Cell Biol.* **153**, 1175 (2001).

⁶¹B. Isralewitz, M. Gao, and K. Schulten, *Curr. Opin. Struct. Biol.* **11**, 224 (2001).
⁶²A. E. Filippov, J. Klafter, and M. Urbakh, *Phys. Rev. Lett.* **92**, 135503 (2004).